Development and cytocompatibility study of hydroxyapatite-hydrogel porous composite scaffold: A potential material for soft and hard tissue regeneration

A Thesis Submitted

In Partial Fulfillment of the Requirement for the Degree of

Master of Engineering

In

Biomedical Engineering

Affiliated to
Faculty of Engineering and Technology
Jadavpur University
By

Swapno Chanda

Examination Roll No- M4BMD19004
University Registration No-123839 of 2013-14

Under the Guidance of

Dr. Piyali Basak
School of Bio-Science and Engineering,
Jadavpur University

&

Dr. Biswanath Kundu
CSIR-CGCRI , Kolkata-700032

School of Bio-Science and Engineering

Faculty Council of Interdisciplinary Studies, Law and Management
Jadavpur University
Kolkata – 700032

MAY 2019

M.E. (Biomedical Engineering) course affiliated to
Faculty of Engineering and Technology
Jadavpur University
Kolkata-700032

CERTIFICATE OF RECOMMENDATION

We hereby recommend that the thesis entitled **"Development and cytocompatibility study of hydroxyapatite-hydrogel porous composite scaffold: A potential material for soft and hard tissue regeneration"** carried out under our supervision by Swapno Chanda may be accepted in partial fulfillment of the requirement for awarding the Degree of Master in Biomedical Engineering of Jadavpur University. The project, in our opinion, is worthy for its acceptance.

_____

Dr. Piyali Basak

(Advisor)
Assistant Professor
School of Bioscience and Engineering
Jadavpur University
Kolkata-700032

_____

Dr. Biswanath Kundu

(Advisor)
Senior Scientist
Bioceramics and Coating Division (BCCD)
CSIR-CGCRI
Kolkata-700032

_____

DIRECTOR

School of Bioscience and Engineering
Jadavpur University
Kolkata-700032

_____

Dean

Faculty Council of Interdisciplinary Studies, Law and Management
Jadavpur University
Kolkata – 700032

M.E. (Biomedical Engineering) course affiliated to
Faculty of Engineering and Technology
Jadavpur University
Kolkata-700032

Certificate of Approval

The forgoing thesis is hereby approved as a creditable study of an engineering subject carried out and presented in a manner satisfactory to warrant its acceptance as a prerequisite to the degree for which it has been submitted. It is understood that by this approval the undersigned do not necessarily endorse or approve any statement made, opinion expressed or conclusion drawn therein but approve the thesis only for the purpose for which it is submitted.

Dr Piyali Basak	**Dr. Biswanath Kundu**
(Advisor)	(Advisor)
Assistant Professor	Senior Scientist
School of Bioscience & Engineering	Bioceramics and Coating Division (BCCD)
Jadavpur University	CSIR-CGCRI
Kolkata - 700032	Kolkata-700032

DECLARATION OF ORIGINALITY AND COMPLIANCE OF ACADEMIC ETHICS

I hereby declare that this thesis contains literature survey and original research work by the undersigned candidate, as part of his **Master of Engineering in Biomedical Engineering** studies during academic session 2018-2019.

All information in this document has been obtained and presented in accordance with academic rules and ethical conduct.

I also declare that, as required by this rules and conduct, I have fully cited and referred all materials and results that are not original to this work.

NAME: Swapno Chanda

EXAM ROLL NUMBER : M4BMD19004

CLASS ROLL NUMBER : 001730201011

THESIS TITLE: Development and cytocompatibility study of hydroxyapatite-hydrogel porous composite scaffold: A potential material for soft and hard tissue regeneration

Signature: **Date:**

ACKNOWLEDGMENT

I would like to express my deepest appreciation to all those who helped me in their own little ways for the completion of this thesis work. Time flies, of course it does. It seems the whole year and my thesis work period just came to an abrupt end in no time at all. Through it all, I would like to express my gratitude to Dr. Piyali Basak, Assistant Professor, School of Bioscience and Engineering, Jadavpur University, Kolkata and Dr. Biswanath Kundu, Senior Scientist, Bioceramics and Coating Division, Central Glass and Ceramic Research Institute (CGCRI), Kolkata whose constant support, invaluable guidance and innovative ideas have steered me through to the end of my work. I find immense pleasure to have had them as my thesis advisors. I am grateful to them for taking me on as a student, for their constant optimism and for having faith in me and my future.

I take this opportunity to thank Dr.Monisha Chakraborty, Faculty, School of Bio-Science & Engineering, for her constant help and support throughout my work.

My special profound thanks goes to Sarmita Sinha, Pranabesh Sasmal, Dr. Howa Begam, Sujan Krishna Samanta, Pratik Das, Tamojit Santra and all my classmates from School of Bio-Science & Engineering for their constant help while carrying out the various experiments. Without them it would have been extremely difficult for me to carry out my study.

I offer my cordial gratitude to Akrity Anand, Itishree Ratha, Arnob Mahato, Dr. Somoshree Sengupta and Anuradha Jana from my BCCD lab in CSIR-CGCRI Kolkata, for their thorough support and constant motivation.

I sincerely thank Scientific Research Laboratory for the extreme help they provided.

I would like to express my heartfelt regards to Dr. Debrupa Lahiri (Associate Professor, Department of Metallurgical and Materials Engineering, IIT Roorkee) and her students Kanike Rajesh and Satish Jaiswal for graciously agreeing to carry out nano-indentation studies of all the samples.

Last but certainly not the least, I owe much to my parents and my brother and would like to thank them from the bottom of my heart for their constant support, help, unconditional love and care without which none of it would have been possible.

I want to thank my father Dr. Abhijit Chanda for constantly guiding me and providing opportunities more than a son could ever ask for or deserve.

Thank you.

Date: 30.5.2019 Swapno Chanda

List of Figures

List of Tables

Table 3.16: Elastic modulus and hardness values for 3 different composite preparations

Index

Abstract

The present study focuses on the development and characterization of three biodegradable hydrogels and loading them into porous Hap. The polymers were prepared using various chemicals and optimizing the process parameters. All the three polymers, developed in the process, were biodegradable in nature. The extent of biodegradation was verified using SBF and it was found that the rate of biodegradation was different in each case. Phema-pAam Hydrogel showed slow biodegradation while the other two cases, the degradation rates were faster. The polymers were characterized through FTIR, TGA-DTA, nano-indentation etc. so as to get a clear idea about their physical and mechanical properties.

Apart from the development of the above mentioned hydrogels, hydroxyapatite powder with fine particle size was prepared through standard wet chemical route. After thorough physical characterization of the calcined powder, which gave satisfactory results, compacts were prepared from it using uniaxial pressing and subsequent sintering at 1250C. Napthalene was used to ensure a porous hydroxyapatite structure with around 45 % porosity. The pellets were characterised with FTIR, XRD etc. and a simple comparison suggests that the purity and crystallinity of calcined phase were retained in sintered form. Porous Hap with good interconnected pores was developed.

Attempts were made to load the hydrogels into the Hap structure. Different methods were tried and after repeated trial and necessary process optimisation, the hydrogels could be successfully loaded. Thermo-gravimetric analysis revealed that successful loading was attained in each case. The hydrogel loaded porous Hap specimens were found to be coated with polymers and it was also evident from the micrographs that polymers in the form of flakes intruded into the pores. Nano-indentation study confirmed that stiffness and hardness of the composites were low and comparable to the corresponding values of hydrogels. Bioactivity studies revealed that mostly biodegradable

materials caused comparatively faster dissolution of those composites over a longer time span. A simple examination further confirmed that both calcium and phosphate ions were continually released from all the compositions and also apatite layers formed over the composites with time. Results of the primary studies hint towards the possibility of using these hydrogel loaded porous Hap as bone regeneration scaffolds in future particularly for cancellous bones.

CHAPTER 1:
INTRODUCTION,
LITERATURE REVIEW, SCOPE OF THE PRESENT WORK, OBJECTIVE

1.INTRODUCTION

New generation biomaterials often focuses on optimal composition and tailored properties so as to mimic the real biological functions as close as possible. Polymers, be it synthetic or natural, resemble the soft tissue after structural and functional augmentation while metals and ceramics (mostly synthetic, though, in few cases, derived from natural sources as well) are used for replacing hard tissues. Though such biomaterials are used in biological systems as soft and hard tissues replacement material, there is still a long way to go regarding accurate resemblance (both structural integrity and functional aspects) of these materials with biological tissues and organs.

To overcome these differences and to mimic real life functionality as much as possible, lot of engineering and scientific techniques have been adopted so far. Preparation of composites with proper functionability is one such approach. The following discussion presents an overview of biomaterials, classification of biomaterials, synthetic composites as biomaterials, their uses and limitations.

Material is anything made of matter, constituted of one or more substances. Sometimes the term "material" is used more narrowly to refer to substances or components with certain physical properties that are used as inputs to production or manufacturing. In this sense, materials are the parts required to make something.

A **biomaterial** is any substance (other than drugs) or combination of substances synthetic or natural in origin, which can be used for any period of time, as a whole or as a part of a system which treats, augments or replaces any tissue, organ or function of the body [1]. Examples of biomaterial

applications are Heart Valve, Artificial Tissue, Dental Implants, Intraocular Lenses, Vascular Grafts, Hip Replacements etc.

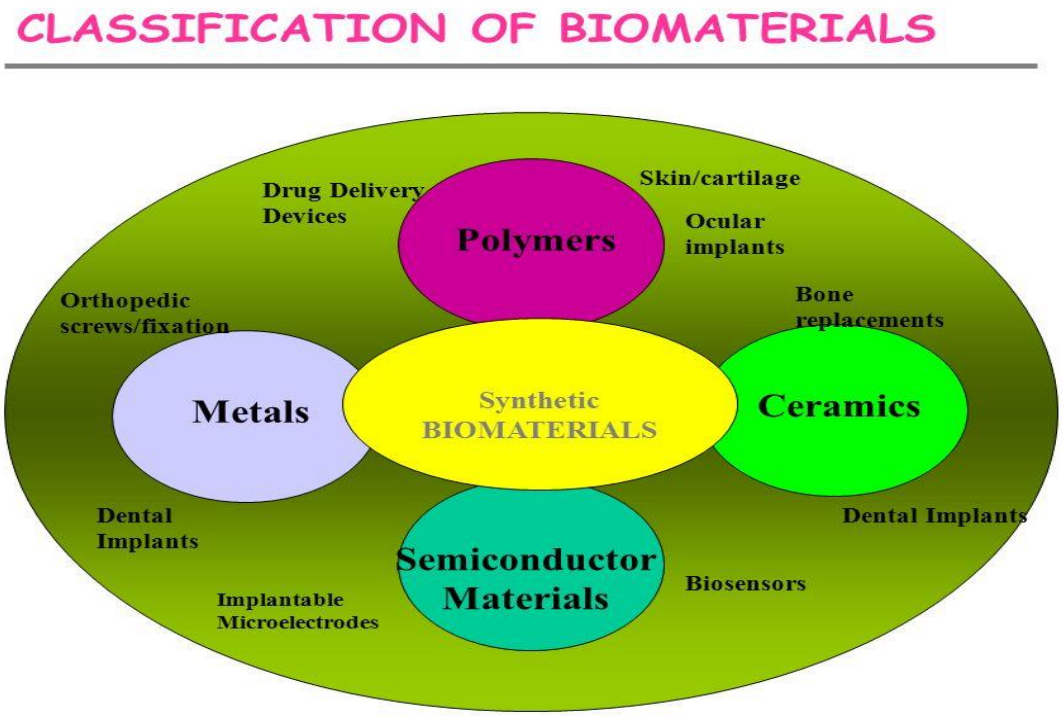

Fig 1.1: Wide Variety of Biomaterials

In another way, we can show the classification in the following format.

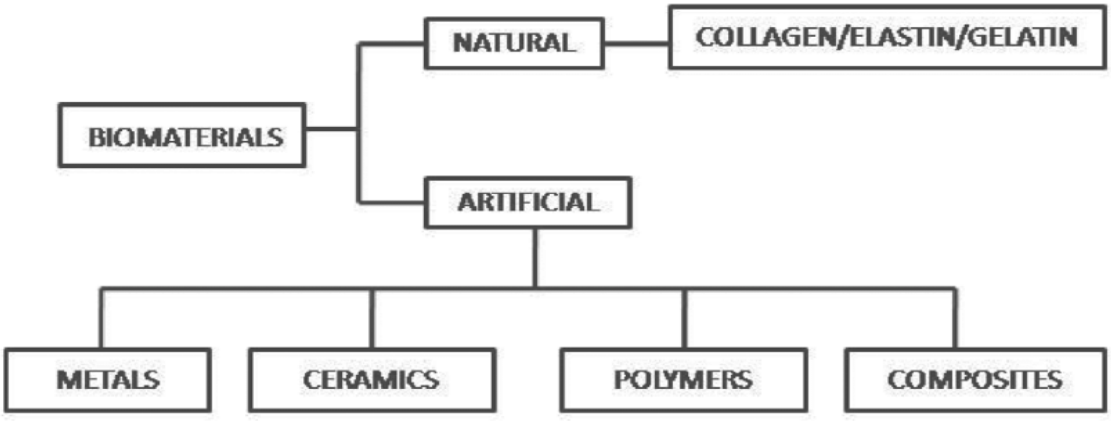

Fig 1.2: Classification of Biomaterials

OVERVIEW OF BIO-CERAMIC MATERIALS

Ceramics used for the repair and reconstruction of diseased or damaged parts of the muscular skeletal system are termed bioceramics. Most clinical applications of bioceramics relate to the repair of the skeletal system, composed of bones, joints and teeth, and to augment both hard and soft tissues.

Table1 .1. Form, phase and function of Bioceramics

Form	Phase	Function
Powder	Polycrystalline Glass	Space-filling, therapeutic treatment, tissue regeneration
Coating	Polycrystalline Glass, Glass- Ceramic	Tissue bonding, Thromboresistance, Corrosion protection
Bulk	Single crystal, Polycrystalline glass, Glass- Ceramic composite (Multi- phase)	Replacement and augmentation of tissue, replace functioning parts.

CLASSIFICATION OF BIOCERAMIC MATERIALS AND ITS TISSUE INTERACTIONS

Implant- An implant is a medical device manufactured to replace the missing biological structure, support a damaged biological structure or enhance the existing biological structure. No material implanted in living tissues is inert, all

implant materials elicit a response from living tissues but the extent varies from material to material. The commonly known effects are mentioned below.

- If the material is toxic, the surrounding tissue dies.
- If the material is non toxic and biologically inactive (almost inert), a non adherent fibrous capsule around the implant forms in order to wall off or isolate the implant from the host.
- If the material is non toxic and biologically active, then tissue forms an interfacial bond with the implant.
- If the material is non toxic and dissolves, the surrounding tissue replaces the implant.

Table 1.2: Types of tissues attachment of Bioceramic Prostheses

Type of Implant	**Type of Attachment**	**Example**
1. Nearly Inert	Mechanical interlock (Morphological fixation)	Aluminium oxide, zirconia
2. Porous	Ingrowth of tissues into pores (Biological fixation)	HA coated porous metals
3. Bioactive	Interfacial Bonding with tissues (Bioactive fixation)	Bioactive glasses Bioactive glass-ceramics Hydroxyapatite
4. Resorbable	Replacement with tissues	Tricalcium phosphate Bioactive glasses

Type 1: Nearly inert implant is loaded by cementing the device onto tissues or by press fitting into a defect called morphological fixation such that interfacial movement occurs, the fibrous capsule can become 100 microns thick and the

implant loosens very quickly. This leads to a clinical failure and necessitates revision surgery involving cost and trauma. In last one or two decades it has been observed that the so-called inert bioceramics are not completely inert. They can also draw living cells towards them to adhere, differentiate and proliferate under favorable conditions.

Type 2: The growth of bone into surface porosity provides a large interfacial area between an implant and its host. This method is biological fixation. As porous ceramics and hydroxyapatite coatings on porous metals were developed to prevent loosening of implants and hydroxyapatite coatings also speeds the rate of bone ingrowth into the pores. For porous implants the pores should be at least 100 microns in diameter so hat capillaries can provide blood supply to the ingrown connective tissues. Vascular tissue does not appear in pores lesser than 100 microns. For last two decades various kinds of doped calcium phosphates are also being tried with an objective to promote higher rate of bone-growth.

Insoluble porous materials have been used as carriers for enzymes, antibodies and antigens or as drug delivery because

- Resistance to microbial attack
- pH changes
- Solvent conditions
- Sustain in high temperature
- Packed under high pressure

Type 3: When a bond forms across the interface between implant and the tissues. This is called bioactive interface and this interfacial bond prevents motion between the two materials and mimics the type of interface that is formed when natural tissues repair themselves. This type of interface requires the material to have a controlled rate of chemical reactivity and thus this bioactive fixation is intermediate between resorbable and bio inert behaviour.

All bioactive implants lead to the formation of hydroxy-carbonate apatite (HCA) layer on their surfaces when implanted. The HCA phase is equivalent in composition and structure to the mineral phase of bone.

Type 4: When the rate of change of a bioactive interface is sufficiently rapid the material "dissolves" or "resorbs" and is replaced by surrounding tissues. It leads to regeneration of tissues instead of their replacement.

Thus resorbable materials must have composition that can be degraded chemically by body fluids or digested easily by macrophages. The degradation products must be chemical compounds that are non toxic and can be easily disposed of without damage to cells. Number of options like TCP, BCP are being tried to optimize the degradation rates as per specific requirement.

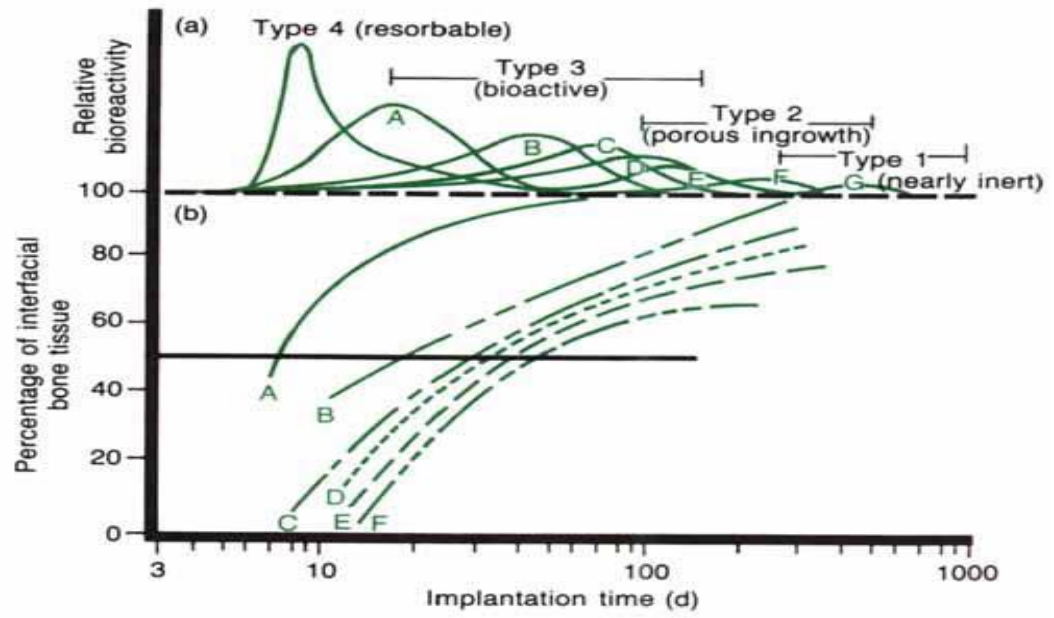

Fig 1.3: Bioactivity spectrum for different bioceramic implants

POLYMERIC BIOMATERIALS

The central role of polymers in the development of functional biomaterials has been fueled in large part by advances in synthetic methodologies that have enabled the production of well-defined and functionalized polymers that are responsive to desired physiological processes. Commonly, synthetic polymers such as poly(hydroxyethyl methacrylate) (PHEMA), poly(lactic-co-glycolic) acid (PLGA), polyvinyl alcohol (PVA), and poly(ethylene glycol) (PEG) have been used widely and for many decades as contact lens and intraocular lens materials, formulated into thin films and microspheres as drug delivery reservoirs, and employed in the preparation of cell-compatible polymer scaffolds for tissue engineering.

With the extensive development of living and controlled polymerizations, additional and numerous types of biomaterials have emerged with increasing levels of sophistication in the ability to tune and manipulate complex physical and biological properties. Ever-increasing functional group tolerance of controlled polymerization methods have enabled a large scope of modifications of polymer behavior (e.g., degradable constituents and biochemical moieties), as well as great flexibility of properties under a wide range of use conditions (e.g., pH, ionic strength, and chemical compounds). The development of recombinant methods as a tool in polymer science has complemented these advances in synthetic methods, and has significantly expanded the library of polymers containing sequences from naturally occurring proteins as well as components of native extracellular matrix (ECM), yielding biomaterials with tailored mechanical and cell signaling functions that mimic the complexity of native tissues.

In designing scaffolds for tissue engineering application, the materials needs to fulfill various criteria such as:- (i) should posses interconnecting pores of appropriate size to enhance the tissue integration and vascularisation, (ii) have controlled biodegradability or bioresorbability so that tissue will eventually

replace the scaffold, (iii) have appropriate surface chemistry to favour cellular attachment, differentiation and proliferation, (iv) possess adequate mechanical properties to match the specific site of implantation and handling, (v) be non-toxic to the biological environment which do not induce foreign response and, (vi) be easily fabricated into various shapes and sizes. The use of three-dimensional (3D) scaffolds provides the framework for cells to attach, proliferate and form extracellular matrix (ECM). Hydrogels have been widely uses as biomaterials due to their unique properties whereby they can form 3D polymer networks that are insoluble, but swell in water and are able to retain a large amount of water within their structures, which is similar to the extracellular matrices (ECM) of many tissues. A major challenge has been the development of hydrogels that have high levels of porosity, whilst maintaining good mechanical properties, as the pore morphology plays an important role in promoting cell growth within the scaffold.

BIODEGRADABILITY

In the design of biodegradable biomaterials, many important properties must be considered. These materials must (1) not evoke a sustained inflammatory response; (2) possess a degradation time coinciding with their function; (3) have appropriate mechanical properties for their intended use; (4) produce non-toxic degradation products that can be readily resorbed or excreted; and (5) include appropriate permeability and processability for designed application. These properties are greatly affected by a number of features of degradable polymeric biomaterials including, but not limited to: material chemistry, molecular weight, hydrophobicity, surface charge, water adsorption, degradation and erosion mechanism. Due to the wide-ranging use of polymeric biomaterials, a single, ideal polymer or polymeric family does not exist. Instead a library of materials is available to researchers that can be synthesized and engineered to best match the specifications of the material's desired biomedical function.

METALLIC IMPLANTS

Metallic materials have predominated in orthopedic surgery, playing a major role in most orthopedic devices, including temporary devices (e.g. bone plates, pins and screws) and permanent implants (e.g. total joint replacements). Concurrently, metals also found applications in dental and orthodontic practice, including tooth fillings and roots. Recently, increasing research effort in metallic biomaterials has been invested in application of the nonconventional reconstructive surgery of hard tissues/organs, such as the application of Nitinol shape memory alloys as vascular stents and the development of new magnesium-based alloys for bone tissue engineering and regeneration.

Table 1.3: Advantages, disadvantages and specific applications of metallic, ceramic and polymeric biomaterials in tabulated form

Materials	Advantages	Disadvantages	Common applications
Metals			
Stainless steels cobalt chromium, titanium alloys	High impact strength, high resistance to wear, ductile, absorption of high strain energy	Low biocompatibility, corrosion in physiological environment, mismatch for mechanical properties with soft connective tissue	Orthopaedic load bearing and fixation devices, dental implants
Pt, Pt–Ir alloys	High conductivity	Low mechanical strength	Neuromuscular stimulation
Ceramics			
Alumina Zirconia	Good biocompatibility, inert, corrosion resistance, high tensile strength	Undesirable surface properties, special techniques are needed for material fabrication	Hip and knee prostheses, dental implants, improving biocompatibility
Calcium phosphate ceramics	Biodegradable	Degradation not controllable	Temporary support, assists regeneration of natural tissues
Polymers			
Polyacrylates, polyesters, polyamides, polyurethanes, polyether, polyolefines, silicone rubber	Low density; easy to fabricate	Low mechanical strength; additives, oligomers may cause tissue reactions	Cardiovascular, maxillofacial, soft skeletal tissue such as tendon, ligament, space filling devices, dental implants, bone cement, lens, intraocular and middle ear prostheses

From the discussions made above, it is evident that there are various kinds of biomaterials, suitable for various purposes but the proper selection of suitable option depends on specific requirements. It is obvious that metals are being used for mostly hard tissue replacement with complicated shapes or applications in case of miniature objects like artificial heart valve, stents etc. while ceramics are used for mostly hard tissue applications like load bearing joints because of their high compressive strength or as coatings. Polymers are more abundant in case of soft tissue applications like skin, cartilage, blood vessel etc.

For real life applications, now it is increasingly being felt that none of the above mentioned varieties in isolation can actually mimic the structure and property of living tissues. So as to resemble the structure and function of the living organs, tissues, it has become almost obvious that combination of materials to form composites is necessary.

1.1 Literature review:

The present chapter deals with the review of relevant research articles on biodegradable biomaterials, with special focus on bone and bone regeneration. These materials do not degrade very fast, rather they are designed to posses an optimal degradation rate. In most of the cases, they provide mechanical support to the tissue (which is damaged and hence to be augmented) and also subsequently get resorbed in the surrounding biological environment when the first purpose is served. But this optimization is often a difficult proposition and requires thorough understanding of the local biological dynamics and the potential of the in-vivo performance of the biomaterial in that environment. A brief review suggests that number of studies have been conducted so far on biodegradable implant materials ranging from Magnesium(Mg)-based metallic implants, Bicalcium Phosphate (BCP) based ceramic implants to biodegradable polymers.

In recent past, a number of research groups have reported the development and biodegradation of magnesium based biomaterials. In the year 2017, M. Haghshenas [2] published a brief yet thorough review article on magnesium based biodegradable implant. He has shown that pure magnesium can corrode too quickly in physiological pH and hence its degradation rate needs to be augmented through addition of alloying elements, surface treatment or through the preparation of metal-matrix composites. In this article, a comprehensive review is provided on different grades of biodegradable magnesium matrix composites . In another article, Lei et al [3] reported the performance of magnesium-hydroxyapatite biocomposite. They reported that apart from good biocompatibility, the composite also possesses good bioactivity, but the resorption rate was poor.

Zheng et.al [4] in the year 2017, reported the biodegradation and the physical, chemical and mechanical properties of tricalcium phosphate-magnesium composites. They also reported about the performance of composites formed

using beta tricalcium phosphate and magnesium-zinc-zirconium composites. They claimed that the dissolution of magnesium ions helped in cell-proliferation to a great extent. It is reported to promote the metabolic activities of osteoblast cells. They reported about the comparative cytocompatibility of various compositions of metal-matrix composites.

In last one or two decades, number of research articles have been published on the biodegradation of calcium phosphate based ceramics. It has been reported that beta-TriCalcium Phosphate (TCP) shows slower degradation than alpha-TCP but later on, an optimal composition of bicalcium phosphate (BCP) was tried [2]. Series of articles have been published on BCP , both in bulk form and coating, involving their physical, chemical, mechanical and biological performances. It has been noticed that in large number of cases the degradation rates were either quite low or not properly optimized. In the process, it was also identified that the route of synthesis, methods of compaction and also the method of composite preparation strongly influence the biodegradation rate and often lead to unwanted generation of particles, macrophage activities and granulomatous tissue formation.

Apart from metals and ceramics, series of polymeric biomaterials have also been tried as biodegradable biomaterials. Seal et al [5] and Yar et.al [6] reported about chitosan-polyvinyl alcohol-polycaprolactone hydrogels which were used to bind heparin and induce angiogenesis. Chitosan being a biodegradable polymer is reported to have good biocompatibility, high charge density and non toxicity. They proposed to use this combination for wound healing.

R. Mohapatra et.al [7] developed polyHema as a novel biodegradable micro porous hydrogel. They did various physical characterizations and studied its biodegradability by introducing microbes into the culture media along with the prepared samples. They verified by examining surface morphology by Scanning Electron Microscopy(SEM) and monitored the rate of biodegradation by carbon

dioxide release method. They reported that the copolymer P(HEMA-co-AA) showed good swelling and optimum biodegradation. They claimed that this material because of its hydrophilic nature and interconnectivity of pores can serve the role of efficient drug delivery systems.

Gkioni et.al [8] in the year 2010, presented a nice, thorough study on mineralization of hydrogels for bone regeneration. It was reported that incorporation of calcium phosphate based ceramics and bioglass into hydrogel matrices can induce bone regeneration. Another alternative, as reported by them, is to create nucleation sites for calcification of hydrogels. They proposed certain systematic steps like soaking of hydrogel with calcium phosphate saturated solutions, incorporation of enzymes that catalyze the deposition of bone minerals and incorporation of synthetic analogues to matrix vesicles that are the initial sites of biomineralisation. They also reported about the biomimetic methods. It seems to be worth mentioning that this review paper is one of the first reports made in 2010 where biodegradable polymers/ hydrogels are reported to possess good potential to serve hard tissue regeneration. Before that, majority of hydrogels were assumed to be only useful for soft tissue replacements. As bone is a highly mineralized tissue, the scope of using hydrogel for its regeneration was thought to be useless before but this article highlighted the scope to a great extent.

Raucci et.al [9] reported a promising approach, based on the combination of sol–gel transition and freeze-drying method, for the development of synthetic fillers to repair and/or regenerate the bone and cartilage defects. The sol–gel method was used to synthesize and maintain the nanoscale Hydroxyapatite precipitates along the gelatin structure, whilst a freeze-drying method was used to lock the structure of the composite. The results demonstrated that the electrostatic interactions between Ca^{2+} ions and COO- groups regulate the alignment of nHA-crystals along the gelatin matrix.

Chang. et.al [10] prepared novel hybrid hydrogels by introducing nano-hydroxyapatite (nHAp) into chitin solution dissolved in NaOH/urea aqueous solution at low temperature, and then by cross-linking with epichlorohydrin (ECH). Their findings revealed that hydroxyapatite nano-particles were uniformly dispersed in chitin hydrogel networks. The chitin/nHAP hybrid hydrogel exhibited about 10 times higher mechanical properties (compressive strength: 274 kPa) than that of chitin hydrogel. Moreover, COS-7 cell culture experiment proved that cells could adhere and proliferate well on the chitin/nHAp hydrogels, suggesting good biocompatibility [10].

Lima et.al [11] fabricated a novel pH-sensitive smart hydrogel for drug delivery applications. Polyvinyl-alcohol (PVA) with polyacrylic acid (PAA) was blended adding synthetic hydroxyapatite (Hap) with freeze-thawed cycles and its effects were studied in terms of mechanical strength, bioactivity, and drug release (theophylline) profile.

1.2 Scope of the present work

From the above mentioned articles (1-11) and the associated other relevant research papers (12-34) , it can be inferred that although different types of biodegradable biomaterials have been tried so far, the extent of success particularly in case of in-vivo models is still not high. In laboratory studies, biocompatibility and biodegradability have been studied for metals, ceramics, polymers, composites but controlled biodegradation of the composites in real life physiological environments is not yet fully achieved. Moreover, the articles, particularly those published in recent past, revealed that biodegradable polymers/ hydrogels are slowly getting considered for fabrication of the hard tissue regeneration scaffolds. Mineralization on hydrogels impregnated with calcium phosphate based ceramics are coming up in a big way and they are claimed to form the basis of new generation biomaterials. But none of the

studies have focused on addressing cortical and cancellous bone regeneration simultaneously. However, often during orthopedic surgery, both cortical and spongy parts suffer loss and hence requires simultaneous replacement.

The present study throws light on this aspect where it is envisaged that composite materials, intended for bone, containing both ceramic and hydrogel can be developed which may act as scaffold for spongy and cortical bone simultaneously. In the present work, attempts have been made to develop three different varieties of Hap-hydrogel composites with different biodegradation rates and to conduct a thorough physical, chemical, mechanical and biological characterizations.

1.3 Objective

1. To develop three different hydrogel compositions with varying swelling and degradation rates.

2. To conduct physical, mechanical characterizations of the hydrogels.

3. To develop hydroxyapatite pellets with high porosity.

4. To develop hydrogel loaded porous Hap pellets through vacuum driven processes.

5. To study the physical, chemical, mechanical, bioactivity and cytocompatibility study of hydrogel-loaded Hap pellets.

CHAPTER 2: MATERIALS AND METHODS

2. Materials and Methods

2.1. Synthesis and Characterizations of three different hydrogel compositions:

2.1.1. Synthesis of Polyvinyl alcohol-Chitosan- Polycaprolactone Hydrogel Film

Materials: Polyvinyl alcohol (mol. Wt.- 72,000) was purchased from Sigma-Aldrich, Chitosan (medium molecular weight) was purchased from Sigma-Aldrich and Polycaprolactone (average molecular weight 80,000) was purchased from Sigma- Aldrich. Deionized water was obtained from a water purification double distillation system.

Fabrication:

- Polyvinyl alcohol (PVA) (0.38g) was dissolved in 7ml double distilled water with vigorous stirring at 80^0 C for 2 hours.
- Chitosan (0.15g) was dissolved in 7ml double distilled water containing 1% acetic acid under stirring for 2 hours at 60 degrees to prepare a solution.
- Polycaprolactone (PCL) (0.072g) was dissolved in a mixture of distilled water, methanol and dichloromethane in a ratio of 0.2:2.8:7 respectively (total 5ml).
- PVA and Chitosan solutions were mixed together for 14 hours, then PCL solution was added and the entire mixture was stirred for 5 hours.
- The mixture was allowed to stand for 30 minutes for removal of air bubbles.
- Finally, the solution was casted on a Petridish and kept in hot air oven at 40^0C for 8 hours.
- The formed film was separated from the Petridish and kept in desiccator for future use.

Fig 2.1: Transparent Hydrogel film as prepared

2.1.2. Synthesis of Polyvinyl alcohol-sodium alginate Hydrogel Film

Materials: Polyvinyl alcohol (mol.wt.-72,000) was obtained from Sigma-Aldrich, Sodium Alginate (91%, Food Grade) was obtained from Loba Chemicals. Also, Glutaraldehyde (GLA) solution (25%, w/w) was supplied by Merck. Deionized water was obtained from a water purification double distillation system.

Fabrication:

- Polyvinyl Alcohol (PVA) (0.8g) was dissolved in 9ml double distilled water by vigorous stirring at 80^0C for 2 hours.
- Sodium Alginate (0.65g) was dissolved in 9 ml double distilled water for 2 hours.
- The two solutions were mixed together for 4 hours.
- 1ml of 2% W/V glutaraldehyde solution was added and mixed for 2 hours.
- The solution was casted on a petridish and kept in hot air oven for water removal for 8 hours at 40^0C.

- ❖ The film was separated from the petridish and stored in desiccator for future use.

Fig 2.2: Hydrogel Film as prepared

2.1.3. Synthesis of Poly(2- hydroxyethyl methacrylate)- Polyacrylamide Hydrogel

Materials: Acrylamide (extrapure), mol. weight 71.08 was purchased from Sisco Research Laboratories Pvt. Ltd. 2-Hydroxyethyl Methacrylate (mol. Weight 130.14) was obtained from HiMedia. Deionized water was obtained from a water purification double distillation system.

Fabrication:

- ❖ 2- Hydroxyethyl Methacrylate (HEMA) (8g), Acrylamide (Aam) (1.6g) and 10.4 ml double distilled water was dissolved together and mixed for 1 hour.
- ❖ The bottle containing the solution was put in Nitrogen purging for 5 minutes, to create an inert atmosphere.

- After nitrogen purging, the bottle was immediately removed and put in gamma chamber.
- Irradiation was carried out at 5kGy dose at a dose rate of 7.63 kGy per hour.
- After irradiation, the hydrogels were scraped out from the bottle with the help of a spatula.
- The hydrogels were washed with running water 3 times a day, for 10 days and dried in hot air oven till constant weight. This was done to remove the unreacted monomers and the uncrosslinked polymers**.**

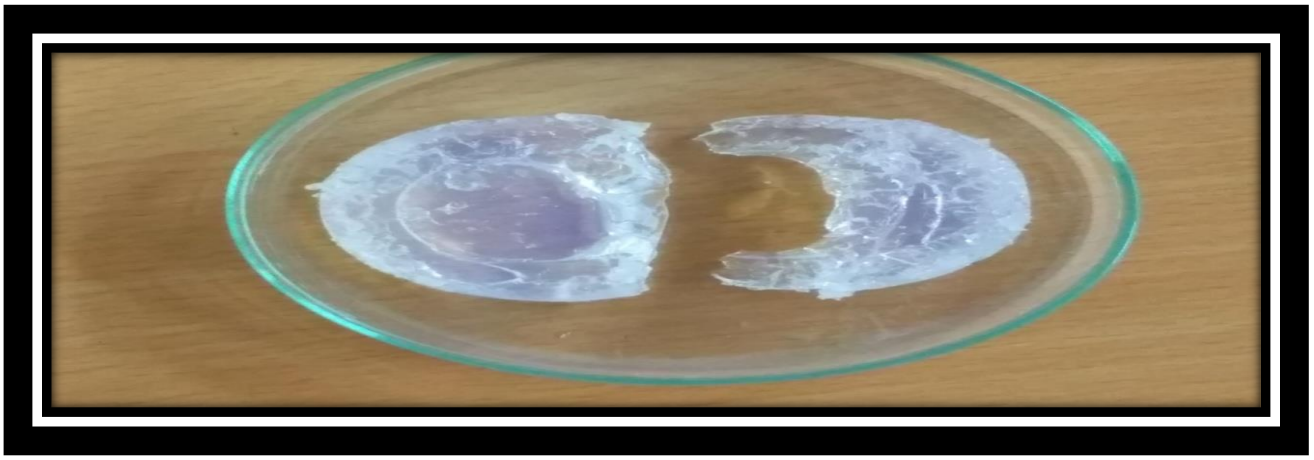

Fig 2.3: Phema- pAam Hydrogel

2.2. Characterizations of the Hydrogels and brief description about technique

2.2.1. Thermo gravimetric Analysis (DTA-TGA):

Thermogravimetry is a technique in which the mass of a substance or changes in physical and chemical properties of sample is monitored as a function of temperature or time, while the substance is subjected to a controlled temperature program. The curve obtained in a TGA is called a thermogram.

Thermal gravimetric analysis is the act of heating a mixture to a high enough temperature so that one of the components decomposes into a gas, which dissociates into the air. It is a process that utilizes heat and stoichiometric ratios to determine the percent by mass ratio of a solute. If the compounds in the mixture that remain are known, then the percentage by mass can be determined by taking the weight of what is left in the mixture and dividing it by the initial mass. Knowing the mass of the original mixture and the total mass of impurities liberating upon heating, the stoichiometric ratio can be used to calculate the percent mass of the substance in a sample.

Working Principle: Sample Holder: Sample and reference are connected by a low-resistance heat flow path. Analyzer usually consists of high-precision balance with aluminium and stainless, platinum sample pans. That pan resides in a furnace and is heated or cooled during the experiment.

Furnace: One blocks for both sample and reference cells.

Temperature controller: Temperature difference between sample and reference is measured. Differential thermal power is supplied to the heaters to maintain the temperature of the sample and reference at the program value.

Sensors: Temperature sensors usually thermocouples and RTD are used

Vacuum requirements: The atmosphere may be purged with an inert gas to prevent oxidation or other undesired reactions.

Analysis is carried out by raising the temperature gradually and plotting weight against temperature. The temperature in many testing methods routinely reaches 1000^0C or greater. After the data is obtained, curve smoothing and other operations may be done such as to find the exact points of inflection. The instrument in thermogravimetry is called a **thermobalance.**

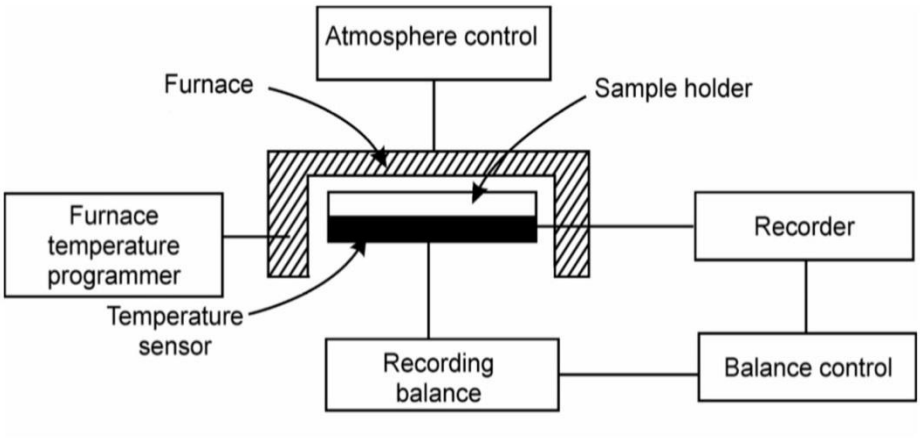

Fig 2.4: Block Diagram of Thermobalance

Differential thermal analysis has been applied in the study of minerals such as clay minerals, carbonates, sulphates and zeolites, sulfides and arsenides, graphite. Thermal analysis instruments predominantly use thermocouples, platinum resistance thermometers, and thermistors. When the sample undergoes a transformation, it will either absorb (endothermic) or release (exothermic) heat.

In differential thermal analysis, the T^{o}C difference between a reactive sample and a non reactive reference is determined as a function of time, providing useful information about the temperatures, thermodynamics and kinetics of reactions. The DTA identifies the temperature regions and the magnitude of critical events during a drying or firing process such as drying, binder burnout, carbon oxidation, sulfur oxidation, structural clay collapse, cristobalite transitions, alpha-beta quartz transitions, carbonate decompositions, recrystallizations, and melting. Thermogravimetric analysis determines the weight gain or loss of a condensed phase due to gas release or absorption as a function of temperature.

The Simultaneous DTA/TGA uses a pan balance, in which the sample and reference cups are supported by a pair of vertical thermocouples (differential thermocouple) positioned on the balance load cell .After both cups are placed

on top of the differential thermocouple stalks, the furnace is lowered over the cups, the balance is zeroed, and the furnace is heated and cooled according to the programmed thermal cycle. The differential thermocouple output (DTA signal) and balance output (TGA signal) are continuously recorded, displayed on a PC monitor, and stored on the PC for post testing analysis.The resulting DTA and TGA curves are simultaneously plotted on a dual Y-axis graph so the DTA's fingerprint and the TGA's weigh loss/gain characteristics are directly compared as the test sample is heated and cooled.

In our study, the TGA-DTA analysis for all samples were performed using **EXSTAR TG/DTA 6300** instrument and temperature range was from room temperature up to 1300^0C at a heating rate of 10^0C per minute. Alumina powder was used as a reference.

2.2.2. FTIR Analysis:

Working Principle: In infrared spectroscopy, IR radiation is passed through a sample. Some of the infrared radiation is absorbed by the sample and some of it is passed through or transmitted. As infrared spectrum represents a fingerprint of a sample with absorption peaks which correspond to the frequencies of vibrations between the bonds of the atoms making up the material. Because each different material is a unique combination of atoms, no two compounds produce the exact same infrared spectrum. Therefore, infrared spectroscopy can result in a qualitative analysis of every different kind of material. In addition, the size of the peaks in the spectrum is a direct indication of the amount of material present. FT-IR refers to a development of IR spectroscopy in which the data is collected and converted from an interference pattern to a spectrum.

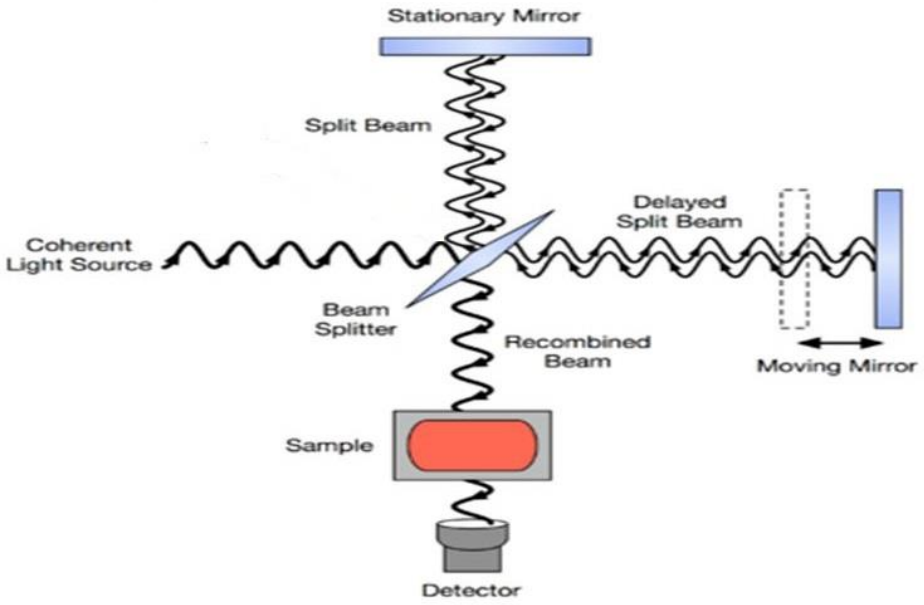

Fig 2.5: Schematic Diagram of FT-IR

In our case, FTIR spectra was taken in the mid IR region (4000-400 cm^{-1}) using KBr discs for all samples except the three hydrogels using **Spectrum 100, Parkin Elmer, U.S.A. instrument**. In all cases, percent transmittance was observed. Bands assignments were carried out from standard databases available.

FTIR spectra of the dried hydrogels were performed using Fourier transform infrared (**ATR–FTIR**) spectrophotometer in attenuated total reflection mode (**IRAffinity-1S, SHIMADZU, Japan**) with a resolution of 4 cm^{-1}. Each spectrum was obtained as average of 32 scans.

2.2.3. X-Ray Diffraction analysis (XRD):

X-rays are electromagnetic radiation with typical photon energies in the range of 100 eV – 100 keV. For diffraction applications, only short wavelength x-rays (hard x-rays) in the range of a few angstroms to 0.1 angstrom (1 keV - 120 keV) are used as it is comparable to the size of atoms and are ideally suited for

probing the structural arrangement of atoms and molecules in a wide range of material. When x-ray photons collide with electrons of the atoms, some photons from the incident beam will be deflected away from the direction where they original travel. If the wavelength of these scattered x-rays did not change, the process is called elastic scattering (Thompson Scattering) in that only momentum has been transferred in the scattering process. These are the x-rays that we measure in diffraction experiments, as the scattered x-rays carry information about the electron distribution in materials. On the other hand, in the inelastic scattering process (Compton Scattering), x-rays transfer some of their energy to the electrons and the scattered x-rays will have different wavelength than the incident x-rays. Diffracted waves from different atoms can interfere with each other and the resultant intensity distribution is strongly modulated by this interaction. If the atoms are arranged in a periodic fashion, as in crystals, the diffracted waves will consist of sharp interference maxima (peaks) with the same symmetry as in the distribution of atoms. Measuring the diffraction pattern therefore allows us to deduce the distribution of atoms in a material. The peaks in a x-ray diffraction pattern are directly related to the atomic distances.

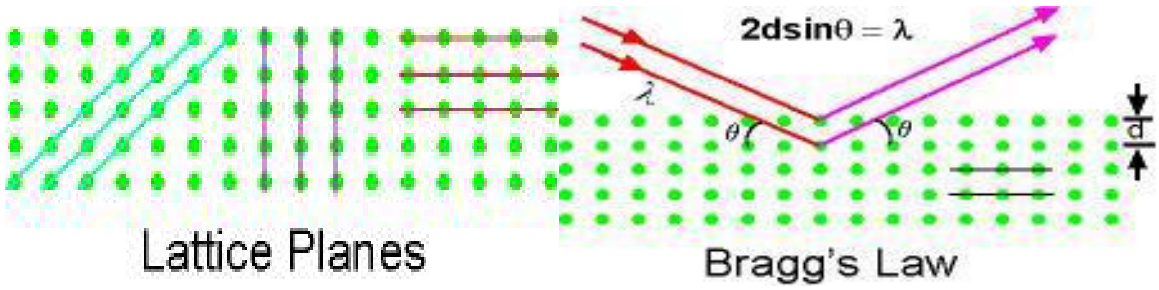

Fig 2.6: Lattice Plane & Brag's Law

For a given set of lattice planes with an inter-plane distance of d, the condition for a diffraction (peak) to occur can be simply written as , $2d\sin\theta = n\lambda$ which is known as the Bragg's law, after W.L. Bragg, who first proposed it. In the

equation, λ is the wavelength of the x-ray, θ the scattering angle, and n an integer representing the order of the diffraction peak.

Powder XRD (X-ray Diffraction) is perhaps the most widely used x-ray diffraction technique for characterizing materials. As the name suggests, the sample is usually in a powdery form, consisting of fine grains of single crystalline material to be studied so that the crystalline domains are randomly oriented in the sample. Therefore when the 2-D diffraction pattern is recorded, it shows concentric rings of scattering peaks corresponding to the various d spacings in the crystal lattice. The positions and the intensities of the peaks are used for identifying the underlying structure (or phase) of the material. Powder diffraction data can be collected using either transmission or reflection geometry, as shown below.

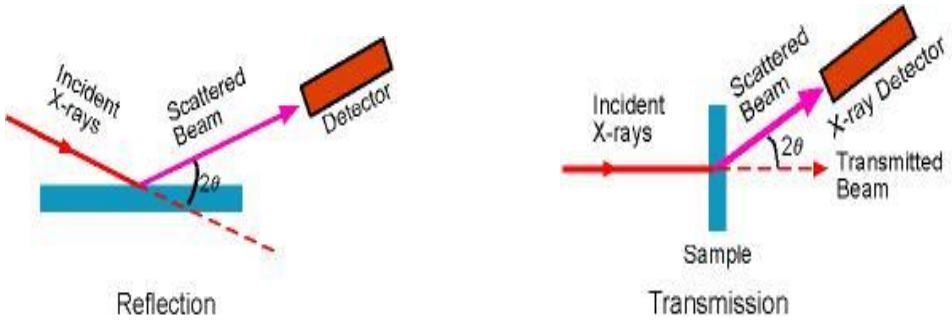

Fig 2.7: Reflection geometry

In this study XRD was done by using **Philips analytical, PW 1710,Netherlands** in 10-80° 2θ(diffraction angle) by continuous scanning for all samples. Phases observed were matched with JCPDS (Joint Committee on Powder Diffraction Standards)

2.2.4. Swelling Study in Stimulated Body Fluid (SBF):

Stimulated Body Fluid: A stimulated body fluid (SBF) is a solution with ion concentration approximately or close to human blood plasma as shown in table below.

The fluid is prepared as described in Kokubo et.al(1990).

Table 2.1: Ion Concentration of SBF and Blood Plasma

Ion	SBF (mM)	Human Blood Plasma (mM)
Na^+	142.0	142.0
K^+	5.0	5.0
Mg^{+2}	1.5	1.5
Ca^{+2}	2.5	2.5
Cl^-	148.8	103.0
HCO_3^-	4.2	27
HPO_4^{2-}	1.0	1.0
SO_4^{2-}	0.5	0.5

Procedure of study: The prepared hydrogel films were cut into small pieces and immersed in SBF (the ratio between weight of the piece and the volume of SBF (pH 7.4) added was kept constant to ensure uniformity). They were kept in incubator at 37^0C. After definite time intervals, they were taken out. The surface was gently wiped with blotting paper and then, weight was measured. Swelling Ratio was calculated as

Swelling Ratio= (Final weight of the sample - Initial dry weight of the sample)/ Initial Dry Weight of the sample

From swelling study, **Degradation percentages** of the films were also calculated. After taking weights of the swollen films, they were kept in oven and dried at 40^0C and weighed again.

Percentage Degradation= (Initial Dry Weight of the film - Weight after drying the swollen film)/ Initial Dry Weight of the film

2.2.5.Nano-Indentation Study:

Nanoindentation test is an effective technique to evaluate the micromechanical properties (elastic modulus, hardness, interfacial adhesion, film fracture toughness) of composites, thin film coatings, polymer materials, soft tissue etc. It works using the same principles as conventional hardness tests, but is performed on a smaller scale using sensitive load and displacement sensing equipment. During the measurement, a sharp indenter of known geometry is projected into the specific site in the material while increasing the load. Both the force and indentation depths are continuously recorded. When it reaches the designated maximum value, partial unloading is performed until the desired depth is attained. Both elastic modulus and hardness can be readily extracted directly from the nanoindentation curve.

According to Oliver and Pharr (O-P) model, which is the most commonly used method to obtain the hardness and Young's modulus of a material by instrumented nanoindentation, the hardness (H) is expressed as:

$H= P_{max}/A_{cr}$ where P_{max} is the maximum applied load and A_{cr} is the real contact area between the indenter and the material.

In this case, the nano-indentation studies were performed using **Hysitron TI 950 Triboindenter** with **Berkovich Diamond indenter with tip size 100 nm.** The loading conditions were **i. Peak Load: 500 μN ii. Loading rate and unloading rate: 50 μN/sec** and **iii. Holding time at peak load: 2 sec.**

2.2.6. Haemocompatibilty Study:

Estimation of Hemocompatibility of the samples is performed through Hemolysis Studies using fresh human blood, collected in a EDTA tube, which was diluted with normal saline solution (2 mL blood + 2.5mL normal saline). A standard sample without sharp edges was kept in a centrifuge tube containing 10 mL of normal saline and was kept in an incubator at 37 °C for 30 min. To this was added 0.2 mL of the diluted blood which was then mixed gently and incubated for 60 min. For the positive control, 0.2 mL of diluted blood was taken in 10 mL of 0.1% sodium carbonate solution and for negative control; 0.2 mL of diluted blood was taken in 10 mL of normal saline solution and incubated for 60 min at 37 °C. In a similar way, sample material was incubated for 60 min at 37 °C. After 60 min of incubation, all the test tubes were centrifuged for 5 min at 4000 rpm and the supernatant was carefully removed and transferred to the cuvette for readings at 545 nm wavelength and percentage hemolysis was calculated.

Percentage hemolysis is calculated based on average of thee replicates.

$$PERCENTAGE\ HEMOLYSIS = [(O.D_{TEST} - O.D_{NEGATIVECONTROL})/(O.D_{POSITIVECONTROL} - O.D_{NEGATIVECONTROL})]x100$$

1. Highly hemocompatible (<5% hemolysis)
2. Hemocompatible (within 10% hemolysis)
3. Non Hemocompatible (>20% hemolysis)

2.3. Synthesis and characterization of Porous Hydroxyapatite Pellets

2.3.1. Synthesis of Hydroxyapatite:

Hydroxyapatite powder was prepared in the laboratory following the standard wet chemical method protocol.

2.3.2.Characterisation of calcined Hap powder:

The calcined Hap powder was subjected to XRD Analysis and FTIR Analysis.

2.3.3. Preparation of porous Hap pellets:

1. The Hap powder, as synthesized, was calcined at 800 degree (5 degrees per minute; and dwelling time 2 hours) to remove the organic (C) components.

2. It was sieved through 50 mesh sieve (300 micron).

3. Naphthalene (Scintillation Grade) powder was taken and sieved using 35 mesh and 70 mesh to obtain particles in the size range 212-500 microns.

4. To prepare Hap pellets of 50% porosity, we mixed 55g Hap and 45g naphthalene and sieved for uniform mixing.

5. For pellet preparation, we took mold of 15mm diameter, 1.25g powder, 200kgf per cm^2 (34.642 MPa), soaking time 1 min.

6. The pellets were subjected to very slow drying with 1 day at 40 degrees, 3 days at 50 degrees and 2 days at 60 degree Celsius for gradual naphthalene removal.

7. Then, they were sintered at 1250 degrees (3 degree per min; and dwelling time 2 hours).

8. An approximate shrinkage of 16.698% (diameter) and 20% (height) was observed after compaction by sintering process and theoretical porosity was 50-55%. (considering pure Hap density – 3.16g/cc)

Fig 2.8: HAp pellets as prepared

2.3.4. Characterization of the prepared porous HAp pellets:

The prepared HAp pellets were subjected to XRD Analysis, TGA Analysis, Apparent porosity and bulk Density measurement and Nano-indentation study.

Bulk Density and Apparent Porosity: The Bulk Density (B.D.) and the percent Apparent Porosity (A.P) of the sintered samples were measured using Archimedes' water displacement method, following ASTM standard(C373) and using the following relationships.

$$B.D = D/(W-S)\ g/cc$$

$$A.P = (W-D)/(W-S)*100\%$$

Where D,S and W are the dry weight, suspended weight and soaked weight of the samples respectively**.**

2.4. Fabrication and Characterization of Hydrogel loaded porous HAp pellets

2.4.1. Loading of PVA-CH-PCL Hydrogel:

Procedure:

1. The solution containing PVA, Chitosan and Polycaprolactone was prepared in the process mentioned before (in the hydrogel preparation section).

2. A preweighed pellet was added to the solution.

3. The solution containing the pellet was allowed to stand for 12 hours.

4. After that, it was put inside dessicator and vaccum of 600mm Hg was applied for 1 hour. It was kept inside dessicator for 18 hours.

5. It was taken out after 18 hours and put inside oven and temperature was maintained at 40^0C.

6. After complete drying, the pellet was separated from hydrogel film and weighed.

2.4.2. Loading of PVA- Alginate Hydrogel:

Procedure:

1. The solution containing PVA, Alginate was prepared as mentioned before.

2. Just after adding glutaraldehyde, a preweighed pellet was added to the solution.

3. The solution containing the pellet was allowed to stand for 12 hours.

4. After that, it was put inside dessicator and vaccum of 600mm Hg was applied for 1 hour. It was kept inside dessicator for 18 hours.

5. It was taken out after 18 hours and put inside oven and temperature was maintained at 40^0C.

6. After complete drying, the pellet was separated from hydrogel film and weighed.

2.4.3. Loading of Phema-pAam Hydrogel:

Procedure:

1. Solution of hydroxyethyl methacrylate and acrylamide was prepared as mentioned before.

2. A preweighed pellet was added.

3. It was put inside vaccum infiltration chamber and infiltration process was carried out for 45 minutes.

4. Immediately after infiltration, the pellet was separated, and put inside gamma chamber for radiation induced copolymerization and crosslinking.

5. Radiation dose- 7.65kGy/ hour, time taken- 55minutes (approx.), Dose- 5kGy.

2.4.4. Physical and Mechanical Characterizations of the loaded composite pellets:

The loaded Hap pellets were subjected to XRD Analysis, SEM imaging, DTA-TGA Analysis, Hemolysis study, Nano-indentation studies.

2.4.5. SEM:

The scanning electron microscope (SEM) uses a focused beam of high-energy electrons to generate a variety of signals at the surface of solid specimens. The signals that derive from electron-sample interactions reveal information about the sample including external morphology (texture), chemical composition, and crystalline structure and orientation of materials making up the sample. In most applications, data are collected over a selected area of the surface of the sample, and a 2-dimensional image is generated that displays spatial variations in these properties. Areas ranging from approximately 1 cm to 5 microns in width can be imaged in a scanning mode using conventional SEM techniques (magnification ranging from 20X to approximately 30,000X, spatial resolution of 50 to 100 nm). Accelerated electrons in an SEM carry significant amounts of kinetic energy, and this energy is dissipated as a variety of signals produced by electron-sample interactions when the incident electrons are decelerated in the solid sample. Secondary electrons and backscattered electrons are commonly used for imaging samples: secondary electrons are most valuable for showing morphology and topography on samples and backscattered electrons are most valuable for illustrating contrasts in composition in multiphase samples (i.e. for rapid phase discrimination).

In our case, microstructural features of the loaded composite samples were observed using Scanning Electron Microscope (**Phenom proX, Phenom-world BV, Netherlands**) equipped with an energy-dispersive x-ray spectrometer (EDX).

2.5. In-Vitro Bioactivity testing and characterization

Bioactivity of the samples were studied through the following tests.

- Weight change in SBF (7,14 days)
- pH change
- apatite layer formation
- Concentration analysis (7,14 days)

CHAPTER 3:
RESULT AND DISCUSSION

3. Results and Discussion

In this chapter the results are presented first followed by an overall discussion at the end. The results are presented in a specific sequence. All results (physical, chemical, biological and mechanical) of three polymer compositions are presented first **(3.1)**, followed by detailed physical characteristics of Hap powder **(3.2)** and unloaded Hap pellet **(3.3)**, and finally all the results on polymer loaded Hap pellets or composites **(3.4)**. A separate portion (**3.5**) deals with bioactivity study done on composites and finally the last portion, marked as **3.6**, presents an overall discussion identifying the major observations.

3.1. Hydrogels

3.1.1. FT-IR Analysis: FTIR data for all hydrogel samples are given below.

3.1.1.1.PVA-CH-PCL hydrogel

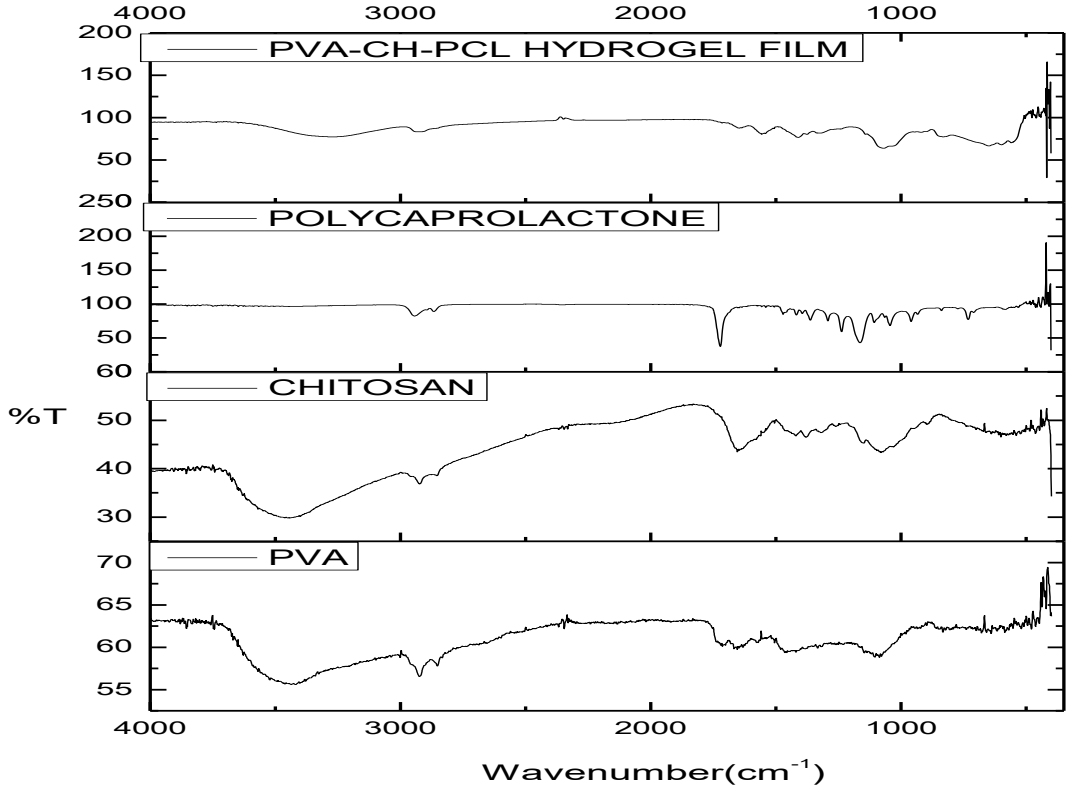

Fig 3.1: FTIR Analysis of PVA-CH-PCL Film along with all components

The following are the peaks obtained for pure PVA, pure Chitosan, polycaprolactone and the prepared hydrogel film in FTIR.

Table 3.1.: Major peaks and assignment for PVA

Major peaks of PVA obtained	**Wavenumber (cm^{-1})**	**Predicted Bonding**
1	2924.48	C-H stretching
2	1085.35	C-O stretching
3	1564.18, 1639.35	C=C stretching vibration
4	3440.38	O-H stretching Vibration

Table 3.2: Major peaks and assignment for Chitosan

Major peaks of Chitosan obtained	**Wavenumber (cm^{-1})**	**Predicted Bonding**
1	3415-34	O-H, N-H stretching
2	2924.48	C-H_2 stretching
3	1639.35	Amide I band
4	1425.17	First overtone of N-H stretching

Table 3.3.: Major peaks and assignment for PCL

Peaks of Polycaprolactone obtained	**Wavenumber (cm^{-1})**	**Predicted Bonding**
1	1727.61	C=O (ester) stretching
2	1163.74	O=C-O-C stretching

Table 3.4: Major peaks and assignment for Hydrogel film

Peaks obtained for PVA-CH-PCL Hydrogel Film	**Wavenumber(cm^{-1})**	**Predicted Bonding**
1	3246-3363	0-H and N-H stretching
2	2928.35	Asymmetric CH_2 stretching
3	1659.63	Amide I band
4	1558.65	C=C stretching
5	1725.61 (small)	C=O (ester) stretching
6	1408.68	O-H bending vibration
7	1057.76	C-O stretching

From the FTIR Analysis, we can conclude that the major peaks of the individual components were present in the hydrogel with slight shifting. This shifting may be the result of bonding and crosslinking among the components.

3.1.1.2 PVA- ALGINATE Hydrogel

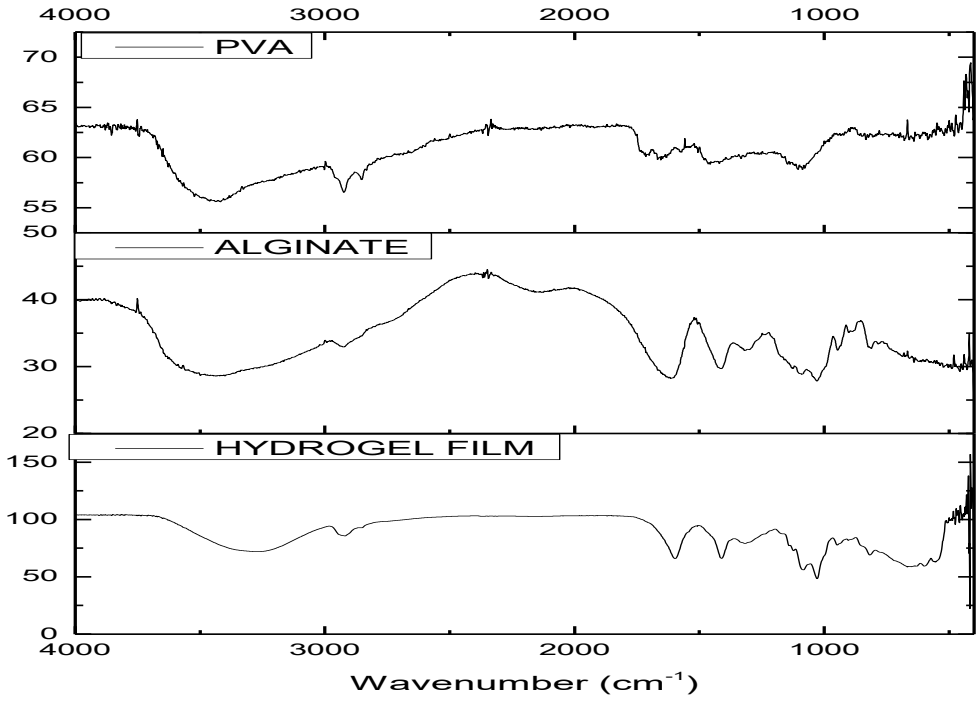

Fig 3.2.: FTIR Analysis of PVA-Alginate hydrogel with each components

The following are the peaks and assignment for Sodium alginate and prepared film. The peaks for PVA have been mentioned before (in case of PVA-CH-PCL hydrogel film).

Table 3.5: Peaks and assignment for Sodium Alginate

Peaks obtained for SodiumAlginate	**Wavenumber (cm^{-1})**	**Predicted Bonding**
1.	2924.48	Asymmetric CH_2 stretching
2.	1602.28	C=C stretch
3.	1412.81	COO^- symmetric stretching
4.	1022.54	C-O stretching

Table 3.6: Peaks and assignment for PVA-Alginate Hydrogel film

Peaks obtained for PVA- Alginate Hydrogel Film	**Wavenumber (cm^{-1})**	**Predicted Bonding**
1.	1599.64	C=C stretch
2.	1407.68	COO^- symmetric stretching
3.	1022.77	C-O stretching
4.	2932.34	C-H stretching
5.	3227-3355	O-H stretching

From the FTIR Analysis, we can conclude that the major peaks of the individual components were present in the hydrogel with slight shifting. This shifting may be the result of bonding and crosslinking among the components.

3.1.1.3. Phema-pAam Hydrogel

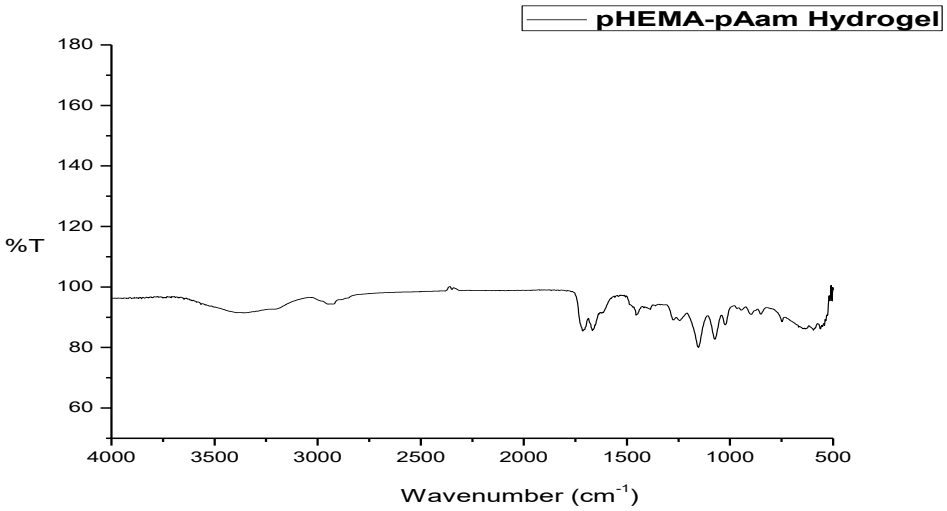

Fig 3.4: FTIR Analysis of Phema-pAam Hydrogel with components

The following are the peaks obtained and their predicted bonding for the hydrogel obtained.

As the gamma rays produced copolymerization and crosslinking of the monomer solutions, we have only taken FTIR Analysis of the hydrogel prepared and have matched peaks with standard FTIR peaks of Poly (2- hydroxyethyl methacrylate) and polyacrylamide.

Table 3.7: Peaks and assignment for Phema-pAam hydrogel

Peaks obtained in Hydrogel	**Wavenumber (cm^{-1})**	**Predicted bonding**
1.	1266	C-C-O stretching
2	1458	C-O
3	1663	C=C stretching, C=O, Amide I band
4	2957	C-H stretching
5	3355	O-H, N-H stretching

3.1.2. Swelling study in SBF

Small pieces of hydrogels were cut from the dried samples, immersed in appropriate amounts of Stimulated Body Fluid (SBF) and were put in incubator at 37^0C. After specific time intervals, samples were taken out, surface wiped gently with blotting paper to remove superficial fluid and weighed.

(Note: In all the 3 hydrogels, for each sample, the ratio of weight of sample to the volume of SBF added was kept constant for non-dimensionalizing the values obtained.

Swelling Ratio (S.R.)=(Weight of the sample after immersion and superficial wiping- Initial Dry weight of the sample)/ Initial Dry weight of sample

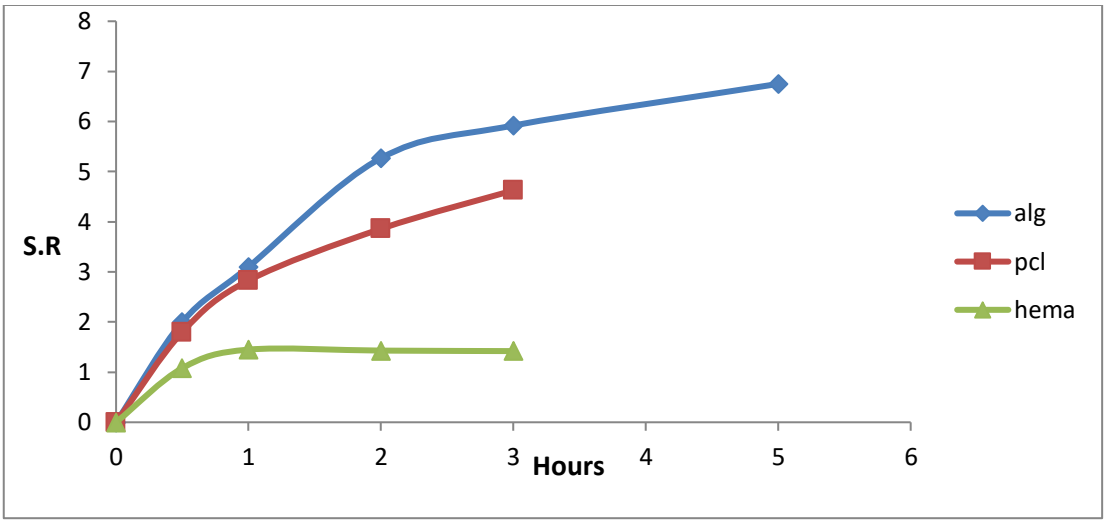

Fig 3.5: Comparative swelling study for the three hydrogels

As we can see from the plot, the rates and extents of swelling (expressed in terms of swelling ratio) for all the three hydrogels were different with PVA-Alginate film showing greatest swelling, followed by PVA-CH-PCL film and Phema-pAam hydrogel respectively.

3.1.2.1. Degradation Study: To get an idea regarding the degradation rate of the three respective hydrogels, we

i. Plotted the swelling ratio versus days graph for the hydrogels for number of days to show the rate of decrease in swelling in them

ii. Plotted the percentage degradation versus days graph by the following formula.

Percentage degradation= (Weight of the initial dry sample- weight of the sample after taking out from immersion in SBF and drying at 40^0C)/ Weight of the initial dry sample

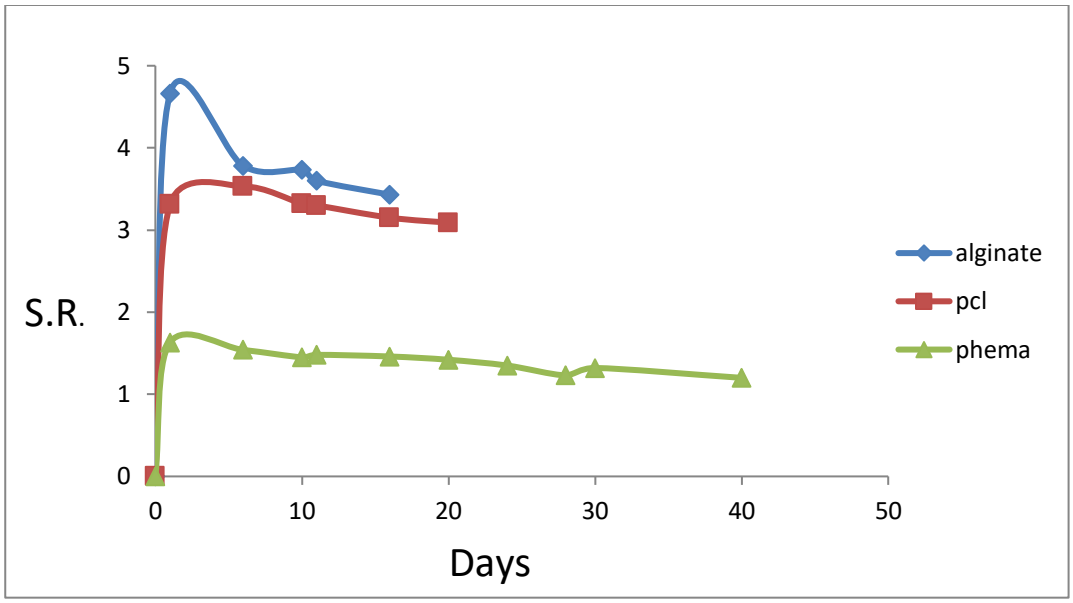

Fig 3.6: Swelling Ratio calculated over days to determine degradation of three hydrogels

As we can see from the plot, the swelling ratio over days for all three hydrogels showed a decreasing pattern, which can corroborate with their degradation kinetics.

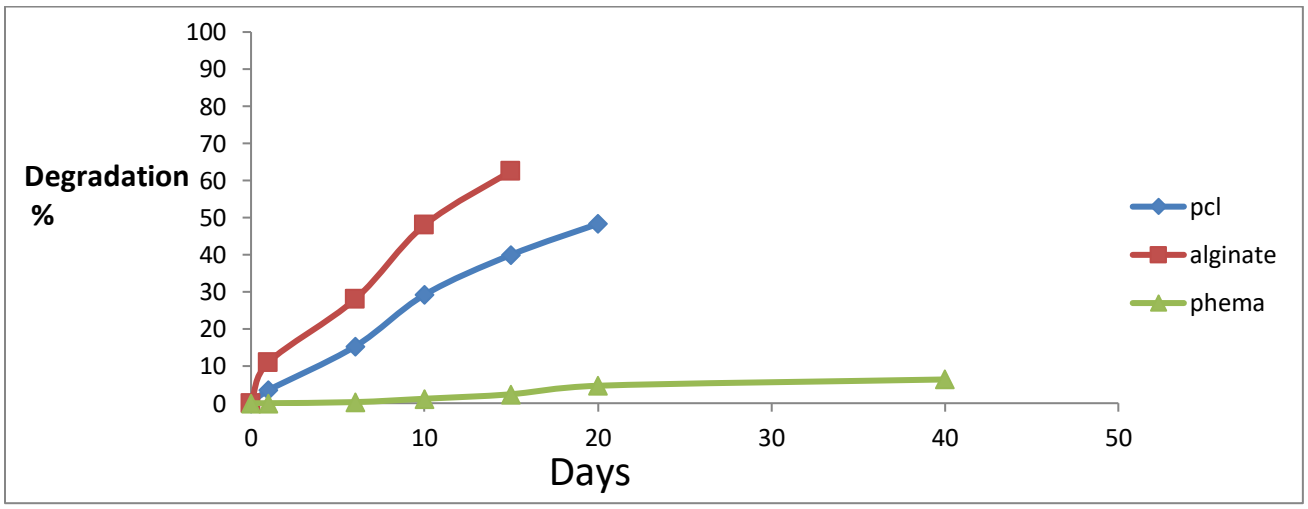

Fig 3.7: Degradation percentage of the three hydrogels over days

Here we have plotted the degradation percentage of three hydrogels over days. Phema-Aam hydrogel showed least degradation while the other two hydrogels showed considerably higher rates of degradation, with PVA-Alginate hydrogel film showing greatest degradation. We can see that for the PVA-Alginate film, almost 60% degradation occurred by 15th day, for the PVA-CH-PCL film degradation was 51% by 20 days whereas for pHema-pAam hydrogel, degradation was less than 10% percent even after 35 days.

3.1.2.2 FTIR of the Hydrogels during Swelling and Degradation studies

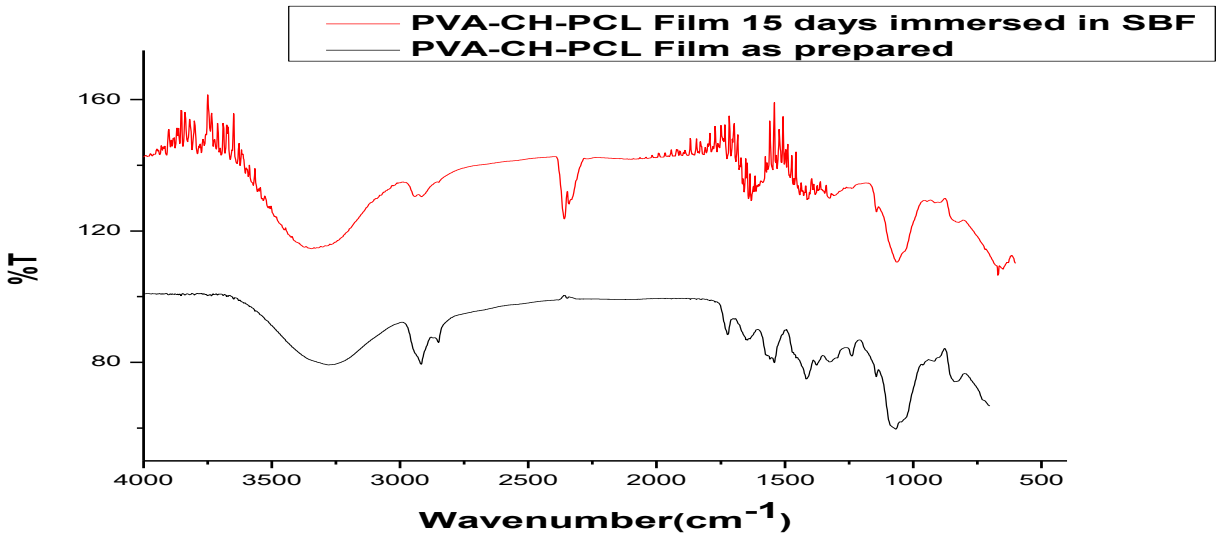

Fig 3.8: Comparative FTIR of PVA-CH-PCL Hydrogel samples i. Sample after preparation and ii. Dried sample after 15 days immersion in SBF

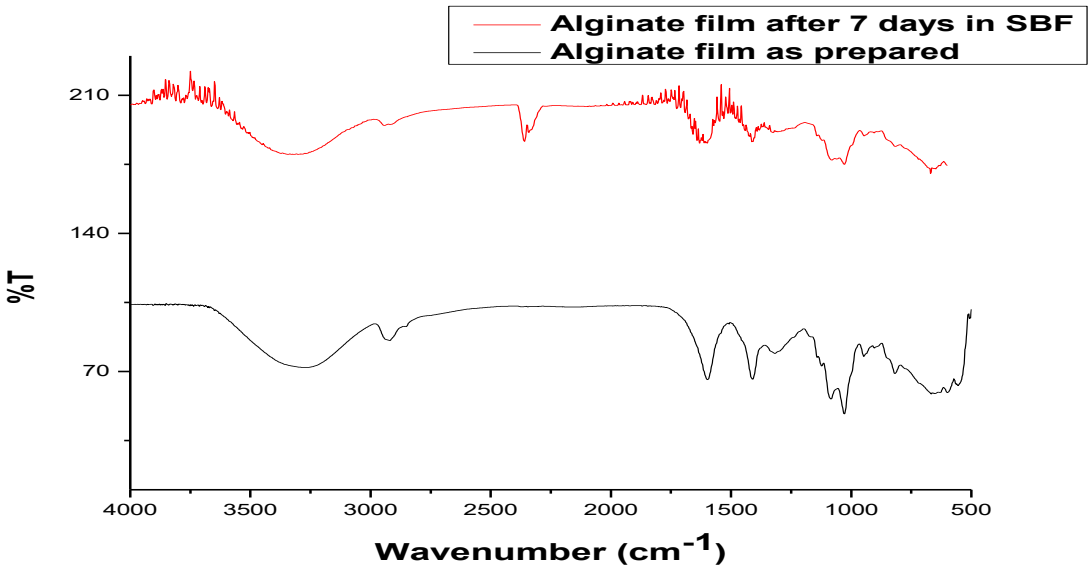

Fig 3.9: Comparative FTIR of Alginate- PVA Hydrogel samples:

i. Sample after preparation and ii. Dried sample after 7 days immersion in SBF

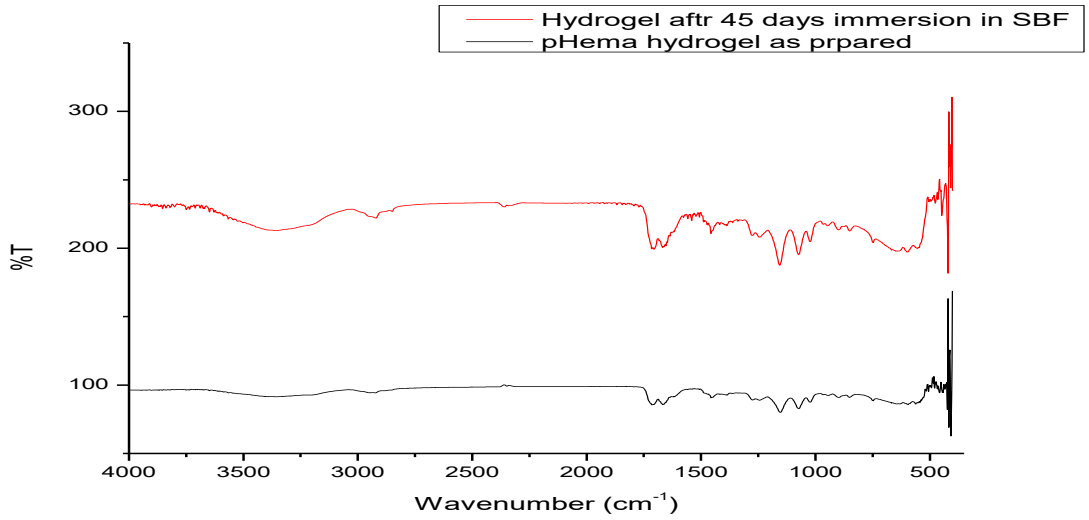

Fig 3.10: Comparative FTIR of pHEMA-pAam Hydrogel samples: i. Sample after preparation and ii. Dried sample after 45 days immersion in SBF

From the above results, we can see that most of the peaks present in the initial samples were present in the samples after swelling. This suggests that no gross degradation took place at the time when these samples were analyzed.

3.1.3. TGA-DTA Analysis

3.1.3.1. TGA-DTA Analysis of PVA-CH-PCL hydrogel sample

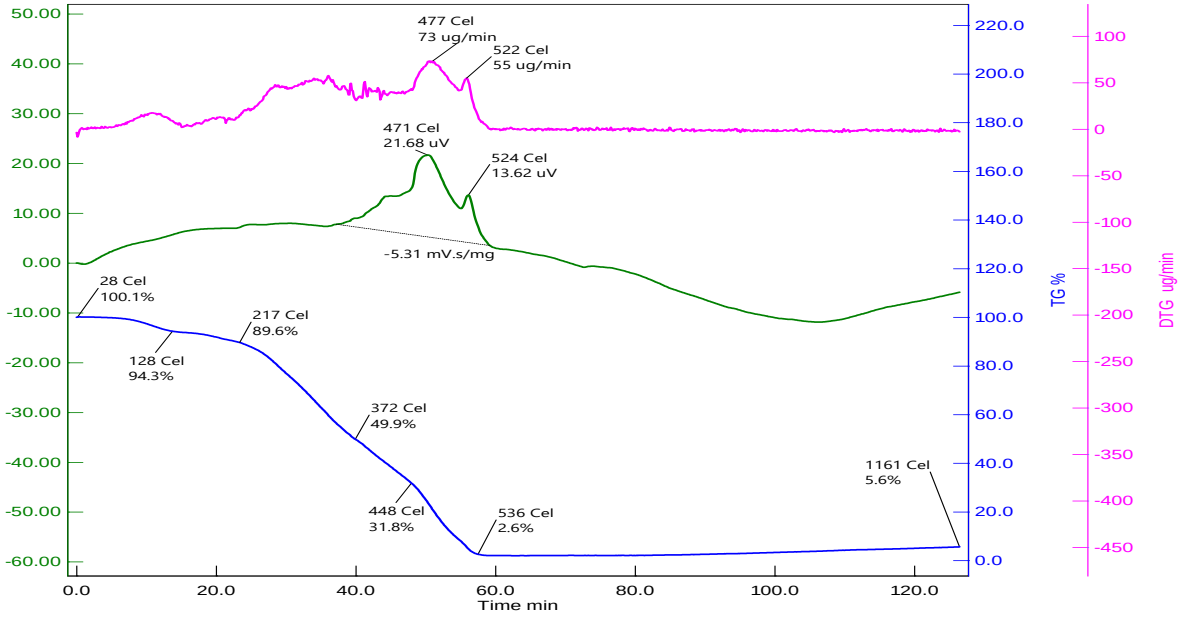

Fig 3.11: TGA-DTA Analysis of PVA-CH-PCL hydrogel sample

We can see that, the mass loss percentage has been plotted with corresponding increase in temperature. As it is evident from the TGA graph, substantial mass loss occurred in the temperature domain of 310-370^{0}C. As far as DTA plot is concerned, there were two sharp endothermic peaks obtained at 471 and 524^{0}C respectively.

3.1.3.2. TGA-DTA Analysis of PVA-Alginate Hydrogel

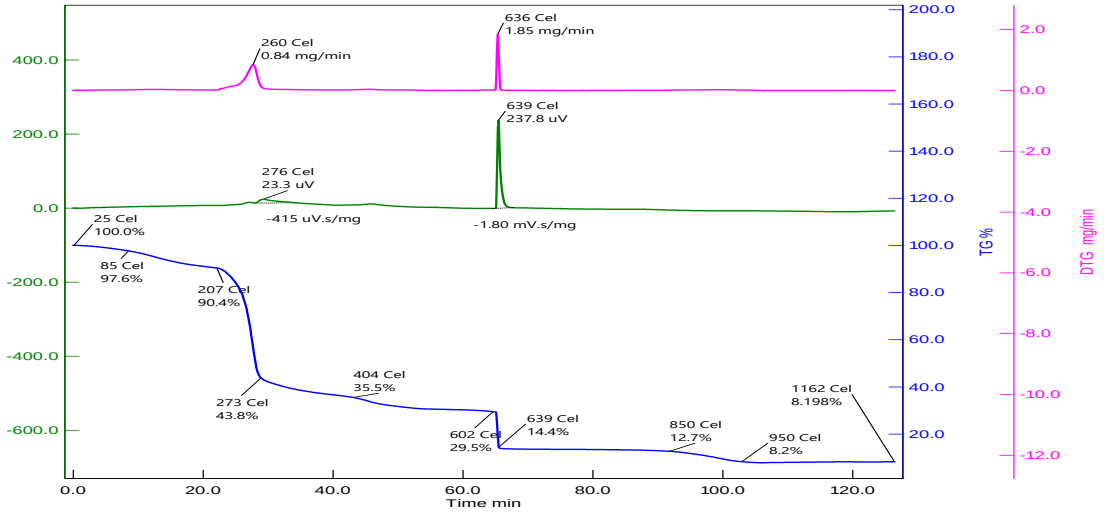

Fig 3.12: TGA-DTA Analysis of PVA-Alginate Hydrogel

We can see that, the mass loss percentage has been plotted with corresponding increase in temperature. As it is evident from the TGA graph, substantial mass loss occurred in the temperature domain of 207-273^{0}C. As far as DTA plot is concerned, there was a sharp endothermic peak obtained at 639^{0}C.

3.1.3.3. TGA-DTA Analysis of Phema-pAam hydrogel sample

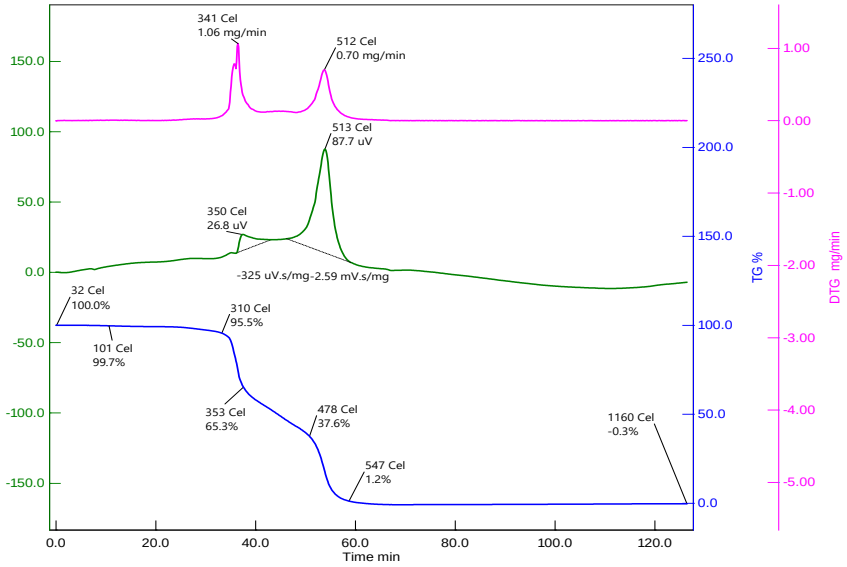

Fig 3.13: TGA-DTA Analysis of Phema-pAam hydrogel sample

We can see that, the mass loss percentage has been plotted with corresponding increase in temperature. As it is evident from the TGA graph, substantial mass loss occurred in the temperature domain of 310-350^{0}C. As far as DTA plot is concerned, there were two endothermic peaks obtained at 350^{0}C and 513^{0}C respectively.

3.1.4. Hemolysis study : the results of all three samples are given below in tabulated form.

Table 3.8: Hemocompatibility data in tabulated form

Hydrogel	**O.D. (TEST)**	**+VE CONTROL**	**-VE CONTROL**	**% HAEMOLYSIS**
PVA-CH-PCL	-0.0161	0.6403	-0.0178	1.1706 (highly hemocompatible)
ALG-PVA	-0.0149	0.6403	-0.0178	1.2906 (highly hemocompatible)
pHema-Aam	-0.0031	0.6403	-0.0178	2.4706 (highly hemocompatible)

From this, it is evident that all the percetage hemolysis values are well below 5%. So we can conclude that all the three samples were highly Hemocompatible.

3.1.5. Nano-indentation study

Loading-unloading curves for three different hydrogels are presented below.

3.1.5.1. PVA-CH-PCL Hydrogel

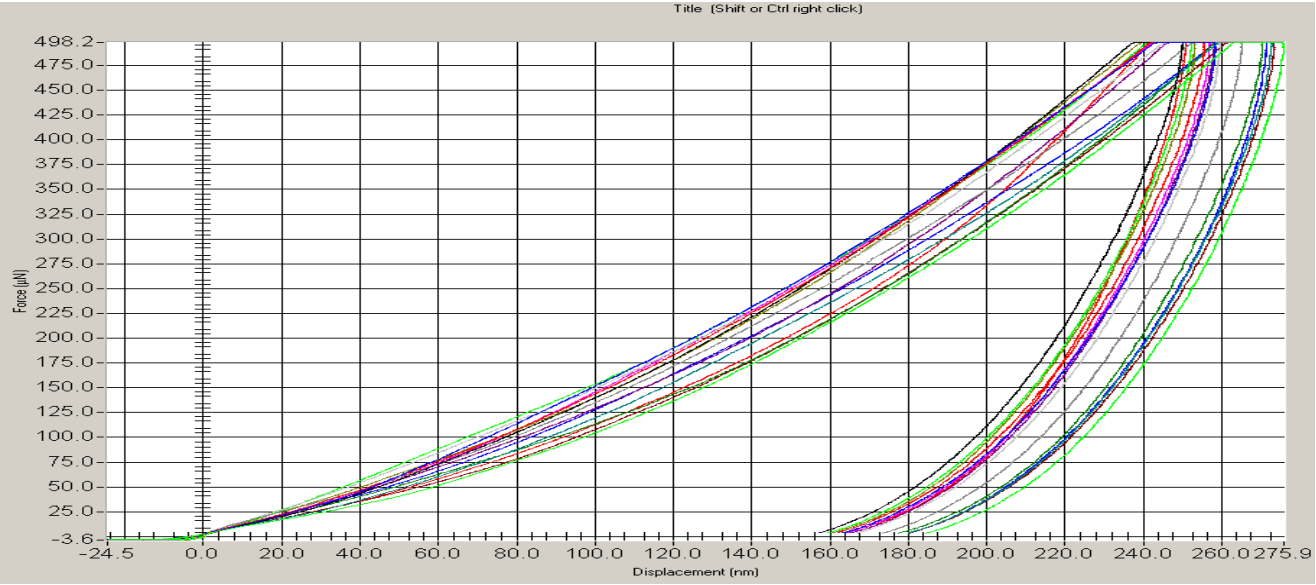

Fig 3.14: Load-Displacement curve of PVA-CH-PCL Hydrogel dried film

3.1.5.2. PVA-Alginate Hydrogel Film

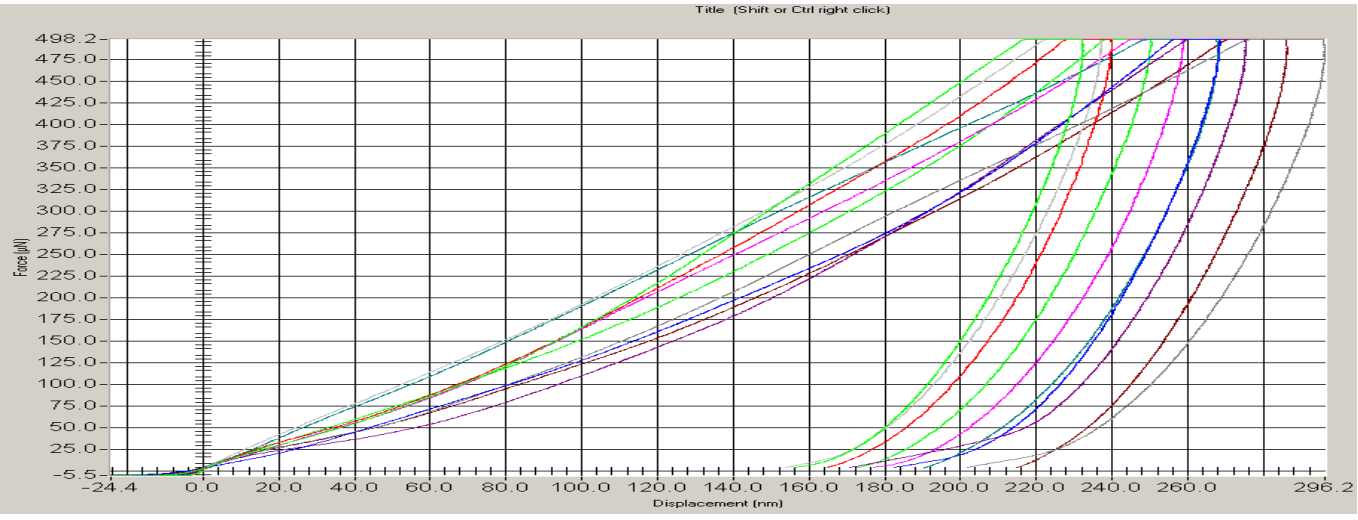

Fig 3.15: Load-Displacement curve of PVA-Alginate dried hydrogel film

3.1.5.3.Phema-pAam Hydrogel

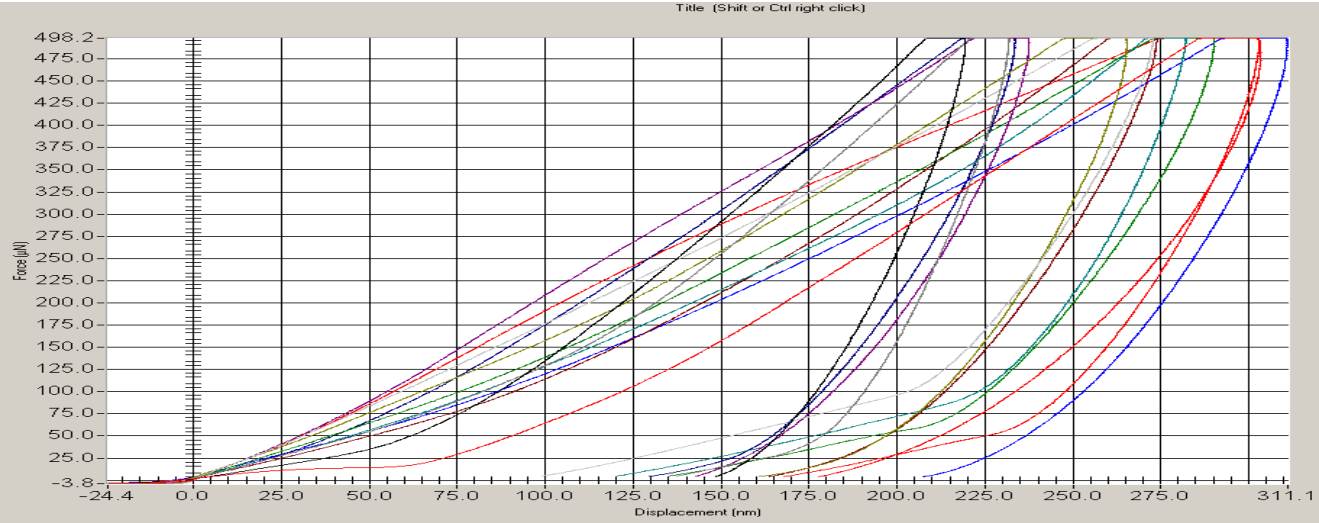

Fig 3.16: Load-displacement curve of Phema-Paam Hydrogel

Table 3.9: Tabulated values of elastic modulus and hardness for the three hydrogels as obtained from the loading unloading curves

Hydrogel	**Elastic Modulus (Gpa)**	**Hardness (Gpa)**
PVA-CH-PCL hydrogel	7.67	0.2964
PVA-ALGINATE Hydrogel	8.96	0.2901
Phema-pAam Hydrogel	7.05	0.2984

None of the loading-unloading curve showed signs of kink formation which clearly denotes that no indentation cracks formed.

3.2. Hap powder testing and results

3.2.1. XRD Analysis

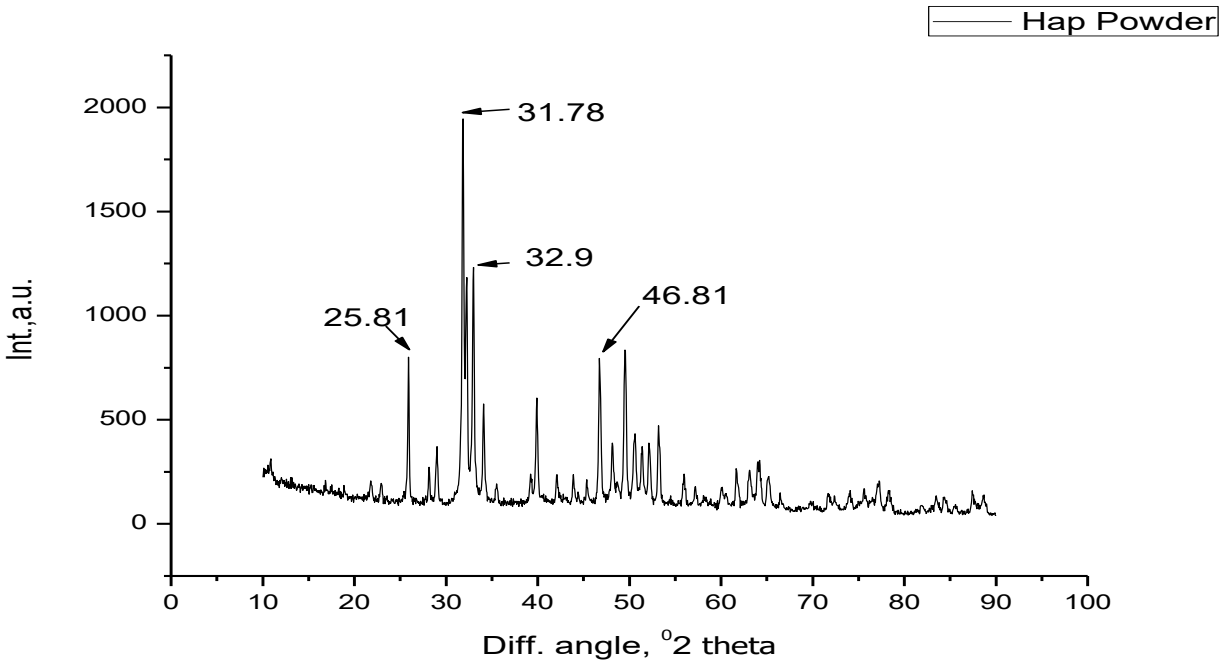

Fig 3.17: XRD Analysis of prepared Hap powder

3.2.2. FT-IR Analysis

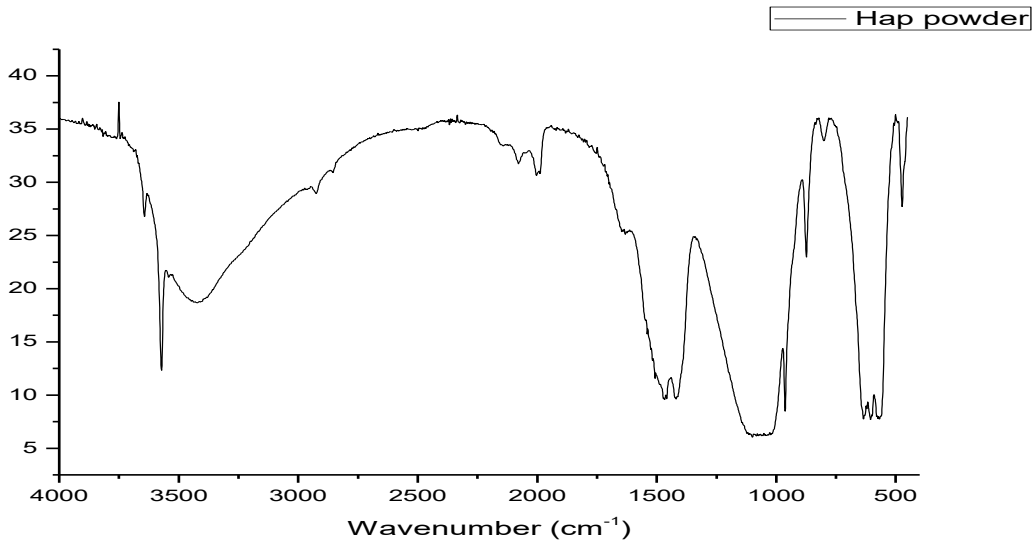

Fig 3.18: FTIR Analysis of prepared Hap powder

Table 3.10: FTIR peaks obtained with assignment in powdered HAp

Peaks obtained from Hap powder	**Wavenumber (cm^{-1})**	**Predicted bonding**
1	1073	PO_4^{-3}
2	1444	CO_3^{2-}
3	3430	OH^-
4	867	HPO_4^{2-}
5	611	PO_4^{-3}
6	791	$P_2O_7^{4-}$

As we can see, all the necessary peaks for Hap powder are present both in XRD and FTIR Analysis. This confirmed the preparation of pure hydroxyapatite.

3.3. Porous HAp pellet tests and results

3.3.1. TGA-DTA Analysis

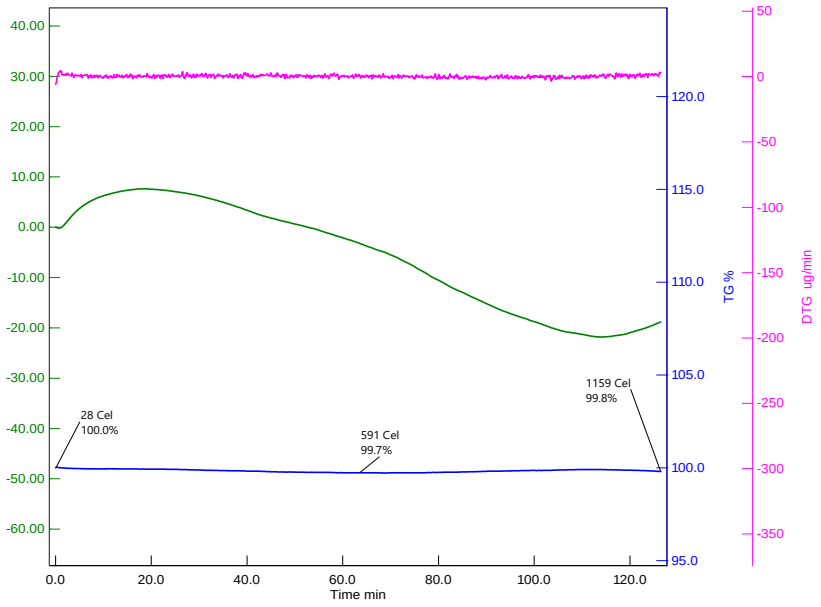

Fig 3.19: TGA-DTA curve for bare HAp pellet sintered at 1250^{0}C at the rate of 3^{0}C per minute

We can see here that as the final temperature attained in TGA was 1150^{0}C, it showed no substantial weight loss as it had been sintered at a much higher temperature (1250^{0}C)

3.3.2. XRD Analysis

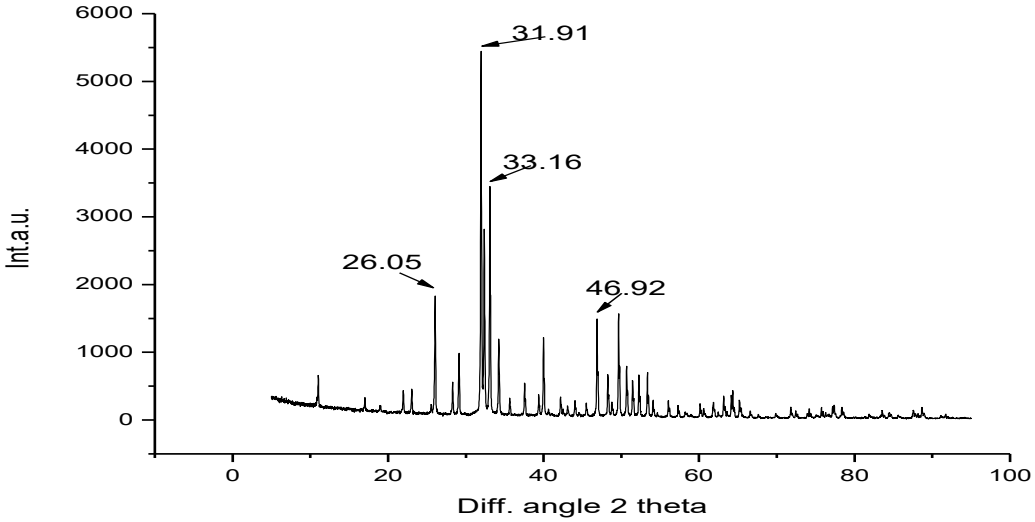

Fig 3.20: XRD Analysis for HAp pellet sintered at 1250^{0}C with the heating rate of 3^{0}C per minute

Table 3.11: Shifting of planes for HAp powder and Hap pellet

Predicted plane	HAp powder	HAp pellet
211	31.7	31.91
112	32.19	33.16
002	25.87	26.05
222	46.7	46.92

As we can see from the given tabulated data, there is a shift in crystalline peaks between the calcined HAp and the sintered HAp pellet. Crystallinity was calculated using standard procedure from the intensity of the peak corresponding to 300 plane and the height of the valley between the peaks

corresponding to 300 plane and 112 plane. For calcined powder, it was found to be 78% while for the sintered pellet, it was 93%.

3.3.3 Apparent porosity and Bulk Density Measurement

Table 3.12: Tabulated data for the Apparent porosity and bulk density measurements of the porous HAp pellets

Suspended Weight(g)	**Soaked Weight (g)**	**Dry Weight(g)**	**Apparent porosity(%)**	**Bulk Density(g/cc)**
0.393	0.752	0.585	46.51	1.634
0.408	0.792	0.610	47.38	1.593
0.502	0.899	0.703	49.37	1.76

As we can see from the data, the porosity of the sintered HAp pellets was found to be consistent, ranging from 45-50%, with corresponding bulk density in the range of 1.6-1.75.

3.3.4. Nano-indentation

Table 3.13: Nano-Indentation results in tabulated form

Material	**Elastic Modulus (Gpa)**	**Hardness(Gpa)**
Bare HAp porous pellet	112.83	6.51

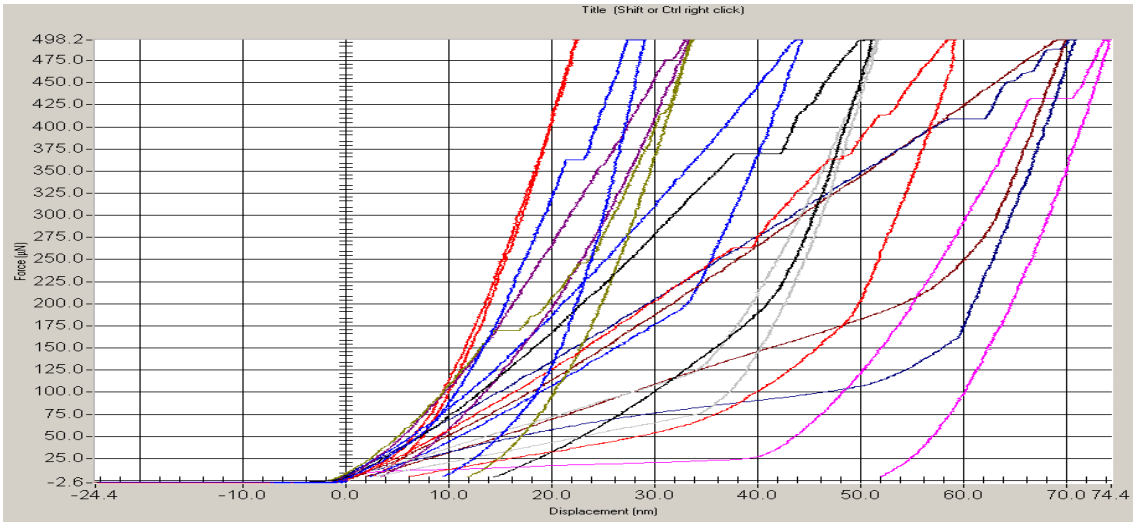

Fig 3.21: Load-displacement curve of porous HAp pellet sintered at 1250^0 C at a rate of 3^0 C per minute

The presence of kinks on number of loading-unloading curves indicate that indentation cracks formed and mostly during loading as expected for a brittle ceramic like Hap.

3.4. Composite characterizations

3.4.1. TGA-DTA Analysis

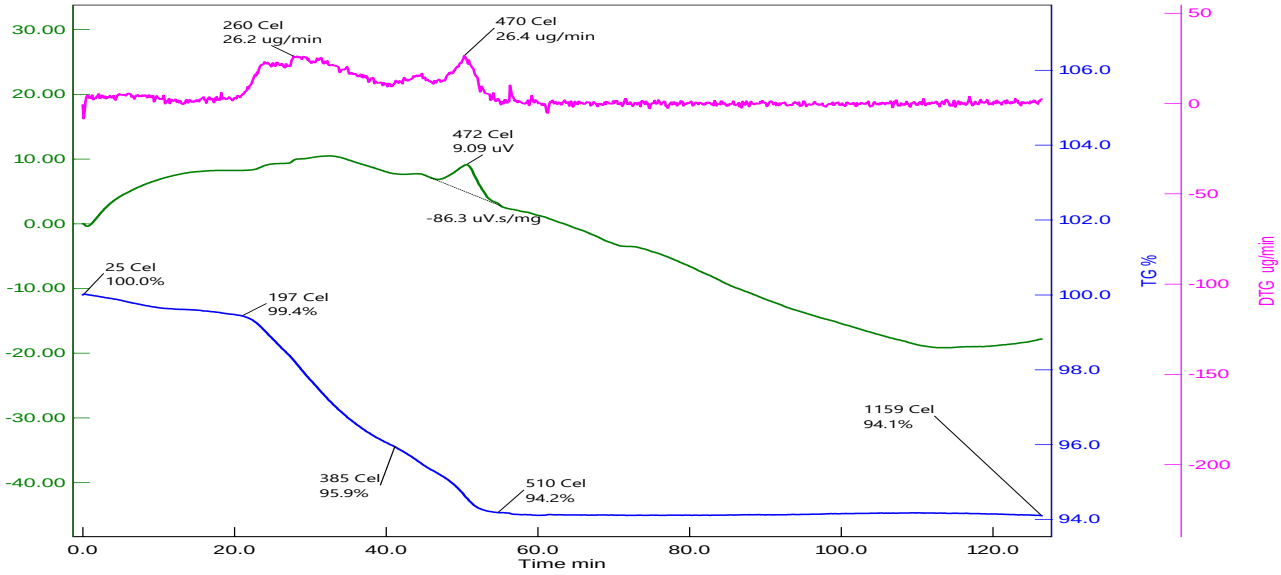

As it is evident from the TGA plot, it is clear that some amount of hydrogel has been loaded into the HAp pellet. From the plot, we can predict an approximate loading (5%) of hydrogel into the pellet.

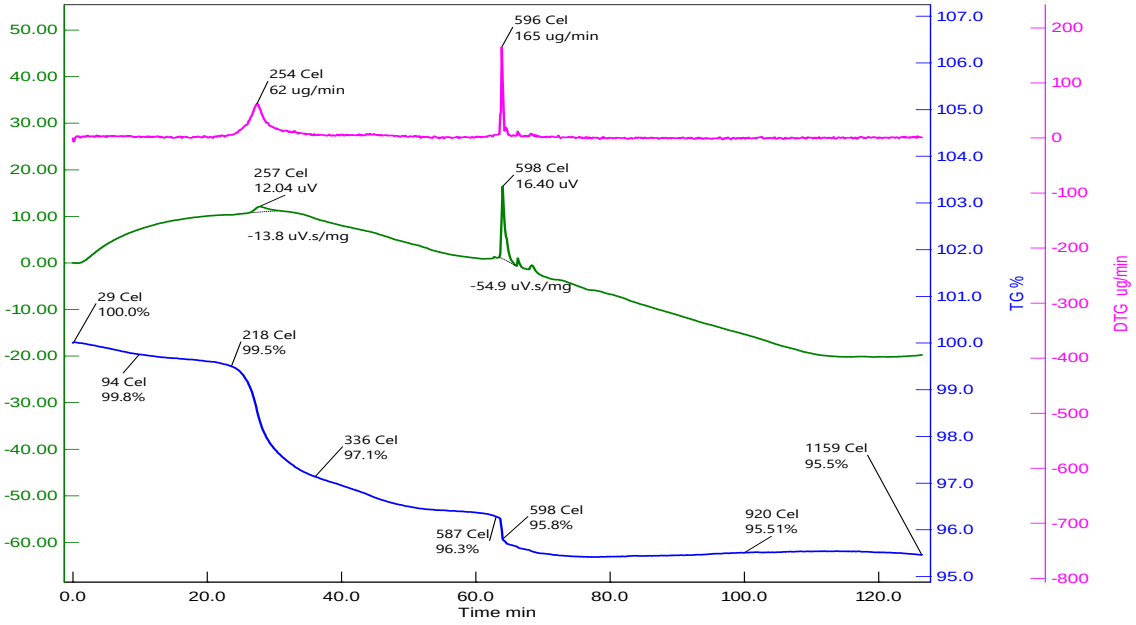

Fig 3.23: TGA-DTA Analysis of PVA-Alginate Hydrogel loaded porous HAp pellet

As it is evident from the TGA plot, it is clear that some amount of hydrogel has been loaded into the Hap pellet. From the plot, we can predict an approximate loading (4%) of hydrogel into the pellet.

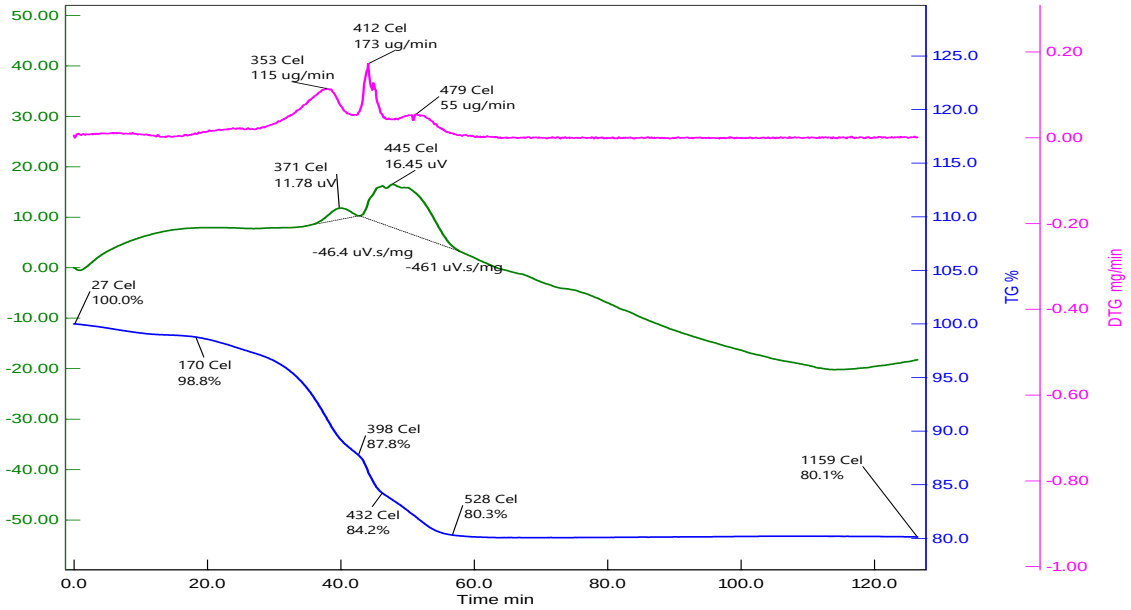

Fig 3.24: TGA-DTA Analysis of pHema-pAam Hydrogel loaded HAp pellet

As it is evident from the TGA plot, it is clear that some amount of hydrogel has been loaded into the HAp pellet. From the plot, we can predict an approximate loading (20%) of hydrogel into the pellet.

3.4.2. XRD Analysis

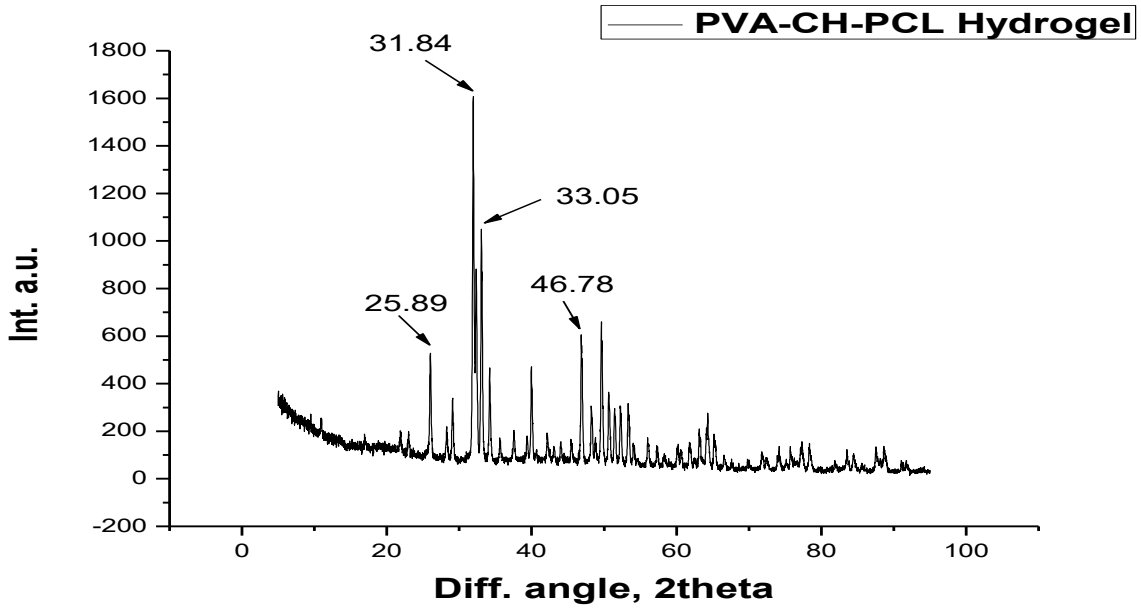

Fig 3.25: XRD Analysis of PVA-CH-PCL Hydrogel loaded HAp pellet

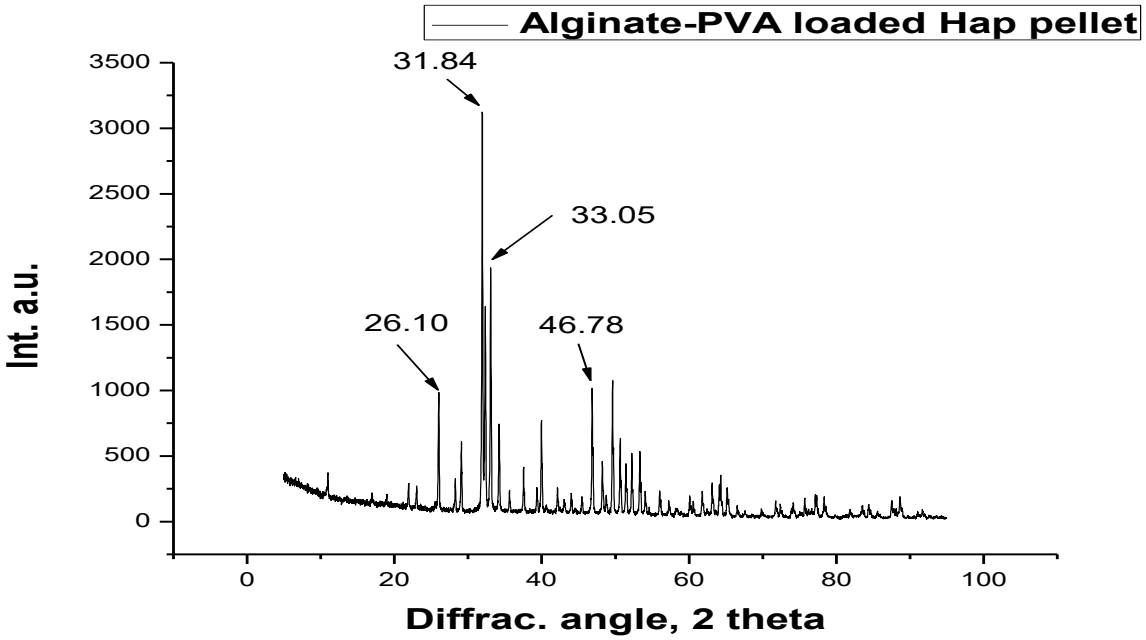

Fig 3.26: XRD Analysis of Alg-PVA Hydrogel loaded HAp pellet

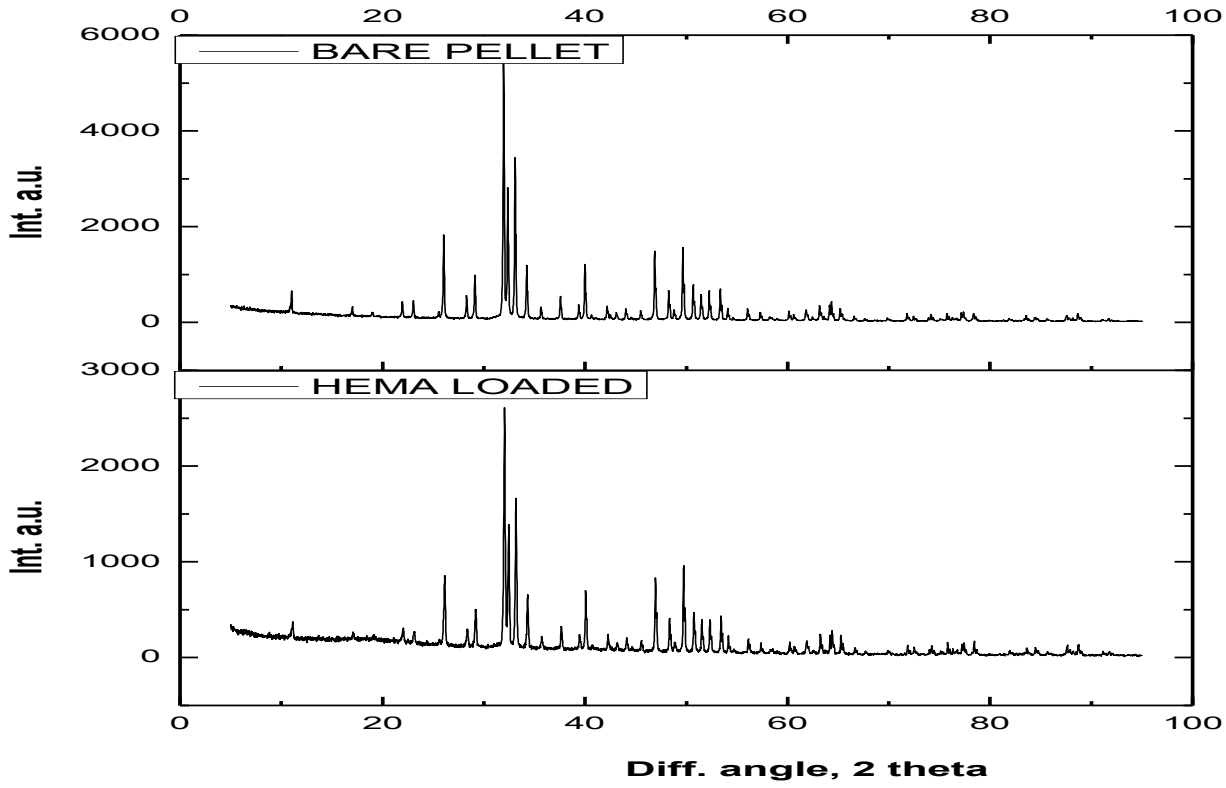

Fig 3.27: XRD Analysis of pHema-pAam Hydrogel loaded HAp pellet

As we can see, there is no major shift seen in the loaded samples compared to that of the unloaded HAp. There is a variation in intensity of some of the crystalline peaks of HAp. We can see an increase in amorphous appearance for the loaded samples because of the amorphous property of the loaded hydrogels. As we are predicting that this hydrogel loading into the HAp pellet is majorly a physical phenomena, we have computed the crystallinity percentage values for unloaded HAp and the loaded composites. The table is as follows.

Table 3.14: Crystallinity percentage comparison

Bare HAp pellet	**PVA-CH-PCL Hydrogel loaded pellet**	**PVA-ALGINATE Hydrogel loaded pellet**	**Phema-pAam Hydrogel loaded pellet**
93%	90%	93%	91%

As we can see, the crystallinity percentage values for the loaded composites don't shift too much from the value obtained in case of sintered unloaded HAp pellet (93%). So, we can say, that the incorporation of hydrogels is majorly a physical entrapment and has no associated gross chemical reaction/ changes.

3.4.3. Hemolysis Study

Table 3.15: Hemolysis study of the composite samples

Hydrogel	**O.D. (TEST)**	**+VE CONTROL**	**-VE CONTROL**	**% HAEMOLYSIS**
PVA-CH-PCL loaded pellet	0.0962	0.8098	0.0238	9.2% (hemocompatible)
ALG-PVA loaded pellet	0.0228	0.8098	0.0238	0.12% (highly hemocompatible)

pHema-Aam loaded pellet	0.0121	0.8098	0.0238	1.4% (highly hemocompatible)

As it is evident from the furnished data, all the composite materials showed hemocompatibility, with the PVA-Alginate and Phema-pAam loaded samples giving slightly better results.

3.4.4. Nano-indentation

3.4.4.1. PVA-CH-PCL loaded HAp pellet

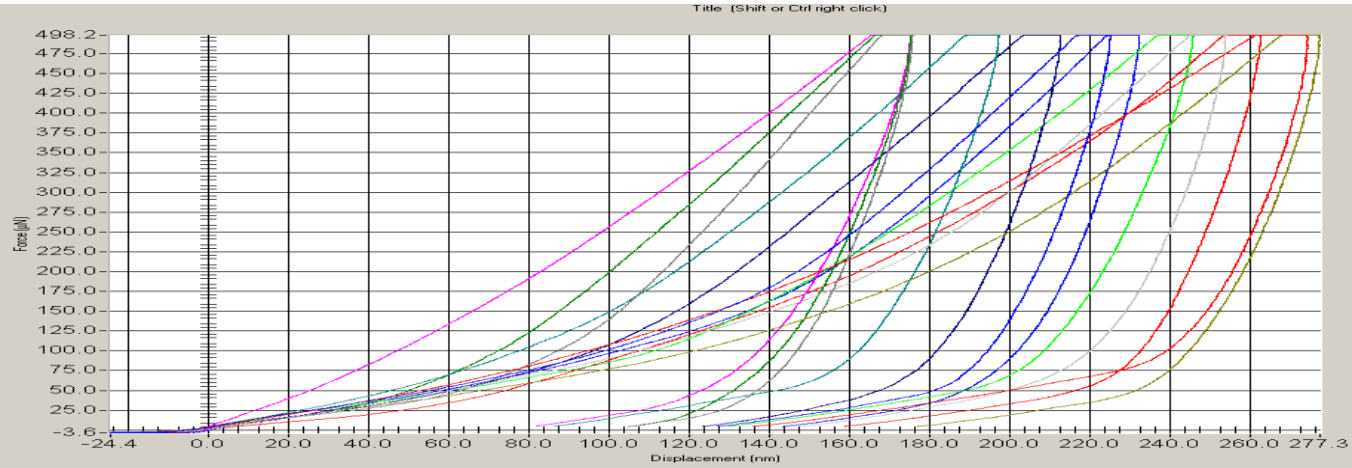

Fig 3.28: Load-displacement curve of PVA-CH-PCL loaded HAp pellet

3.4.4.2. PVA-ALGINATE loaded HAp pellet

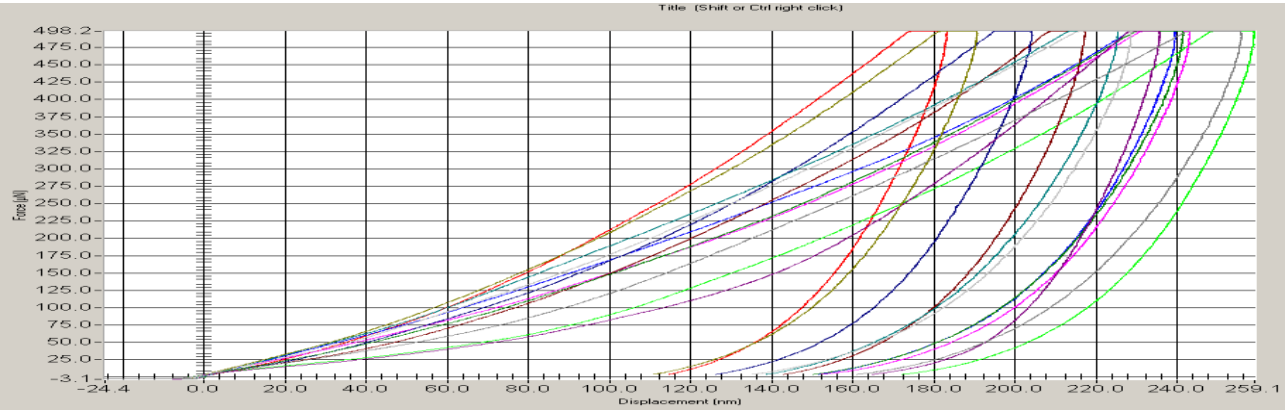

Fig 3.29: Load-displacement curve of PVA-Alginate loaded HAp pellet

3.4.4.3.Phema-pAam hydrogel loaded HAp pellet

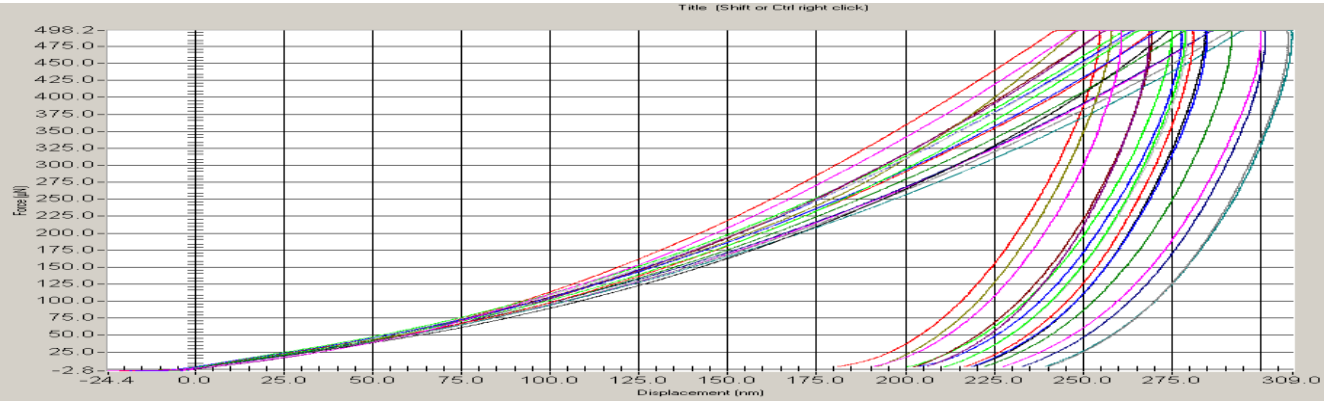

Fig 3.30: Load-displacement curve of Phema-pAam loaded HAp pellet

Table 3.16: Elastic modulus and hardness values for 3 different composite preparations

Composite sample	Elastic Modulus (Gpa)	Hardness (Gpa)
PVA-CH-PCL loaded	14.34	0.4043
PVA-Alginate loaded	11.37	0.3928
Phema-pAam loaded	9.42	0.2383

If we compare the elastic modulus and hardness values of all the samples, we may infer that for the loaded composites, as because the HAp pellets were coated with hydrogel, mainly the effects of the coated hydrogel is showing in the results, associated with a substrate effect, which is the HAp pellet in this case. It may also be noted that most of the loading unloading curves showed no kink formation at all. It hints towards 'no-cracking' which in turn is indicative of more deformability.

3.4.5. SEM micrographs: All the SEM micrographs are placed together (below) to assist effective comparaison between the loaded and unloaded samples.

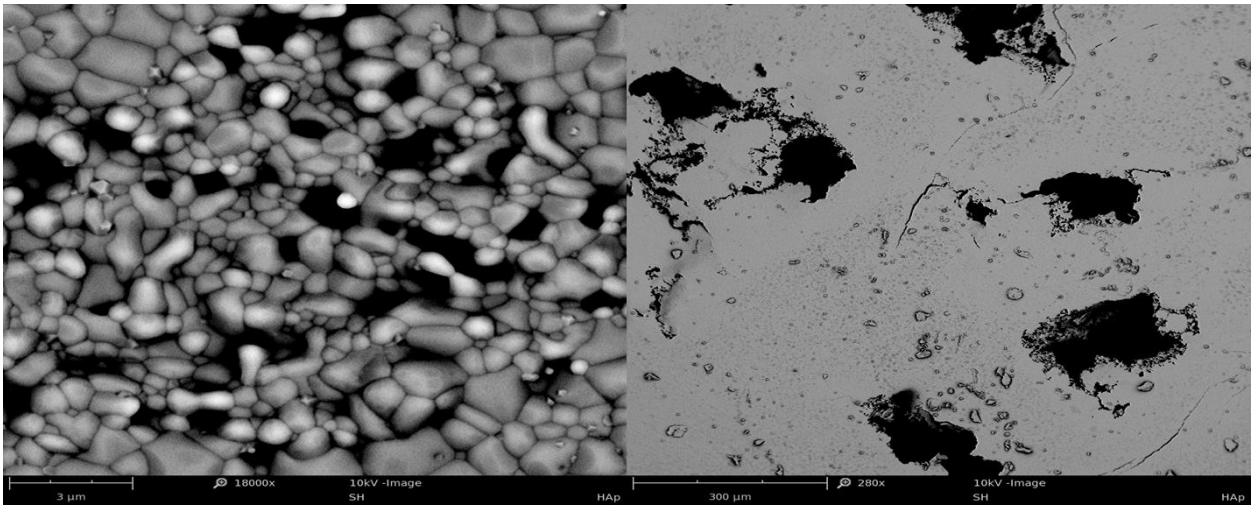

Fig 3.31: SEM micrographs of Bare HAp pellet

From the SEM images, we may infer that pores were non-uniform and sizes varied in the range 200-500 microns.

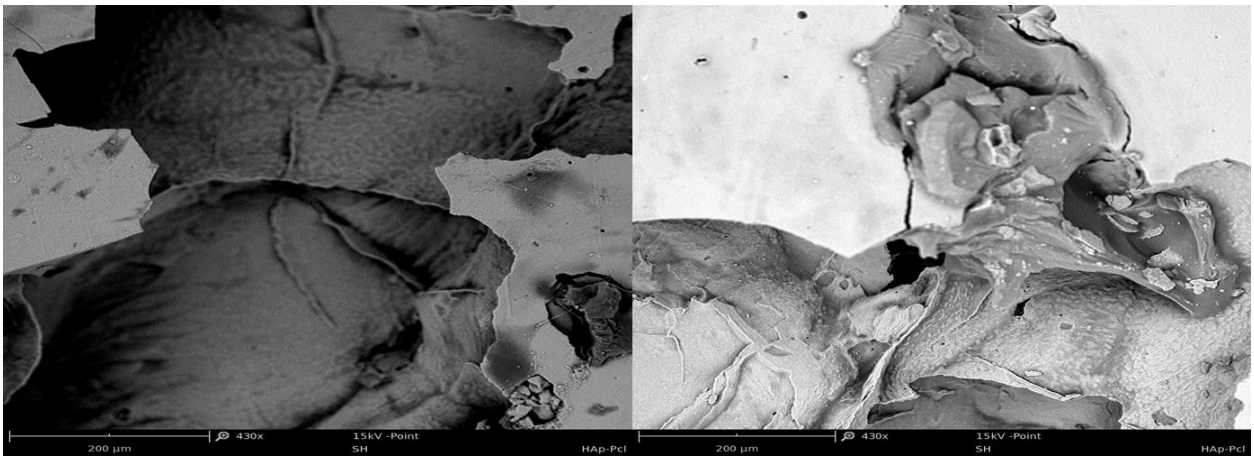

Fig 3.32: SEM micrographs of PVA-CH-PCL-HAp

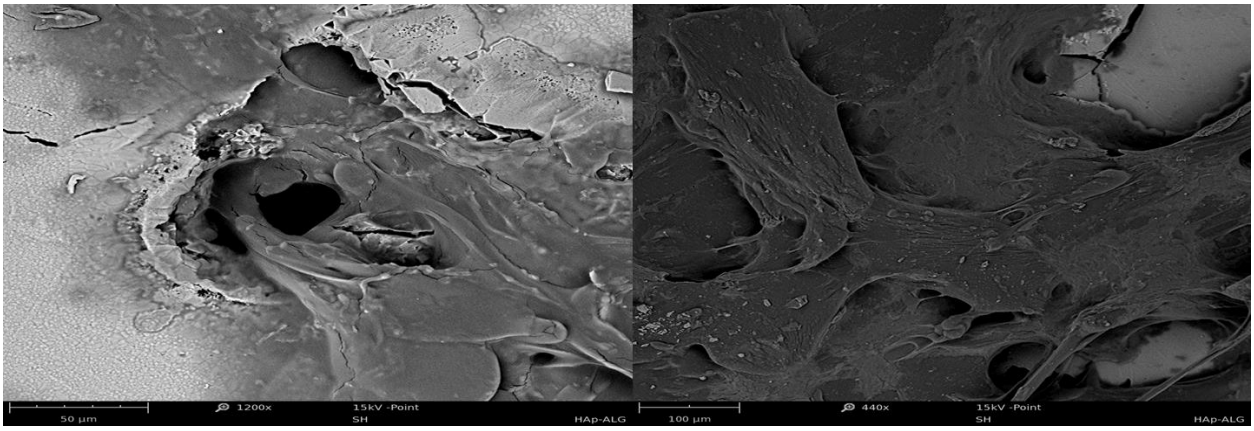

Fig 3.33: SEM micrographs of PVA-Alginate-HAp

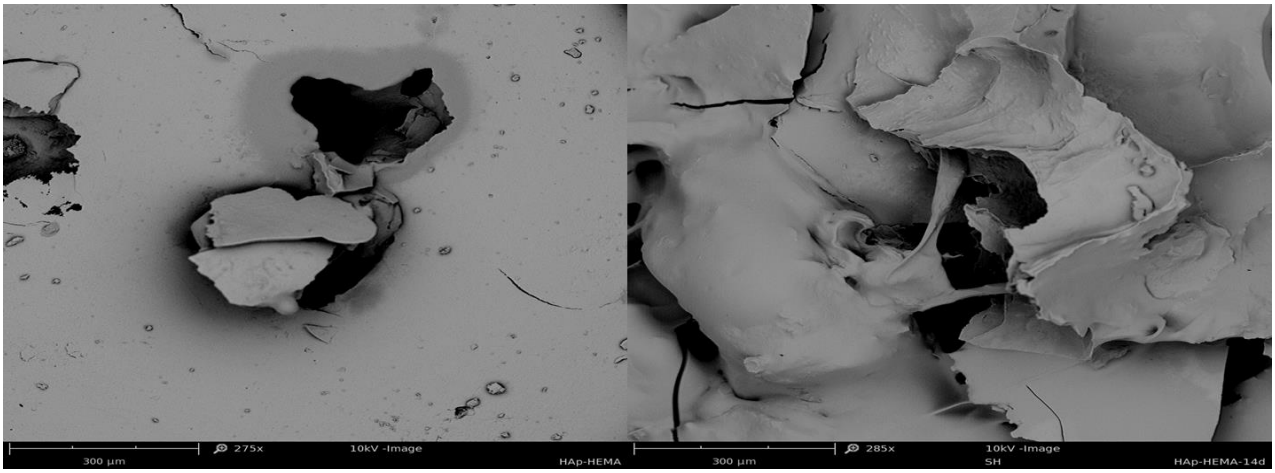

Fig 3.34: SEM micrographs of pHEMA-pAam-HAp

From the SEM images, we can see hydrogel, in the form of flakes in the pores of HAp pellet. This was observed in all three cases and were confirmed through EDXA.

3.5. SBF Bioactivity Study:

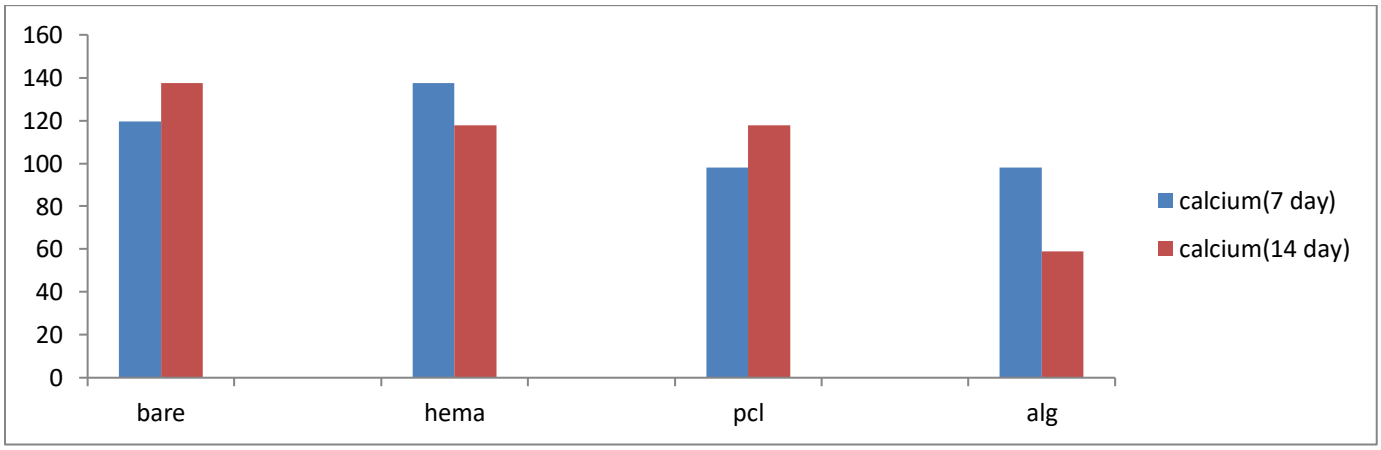

Fig 3.35: Calcium ion concentration in SBF after 7,14 days

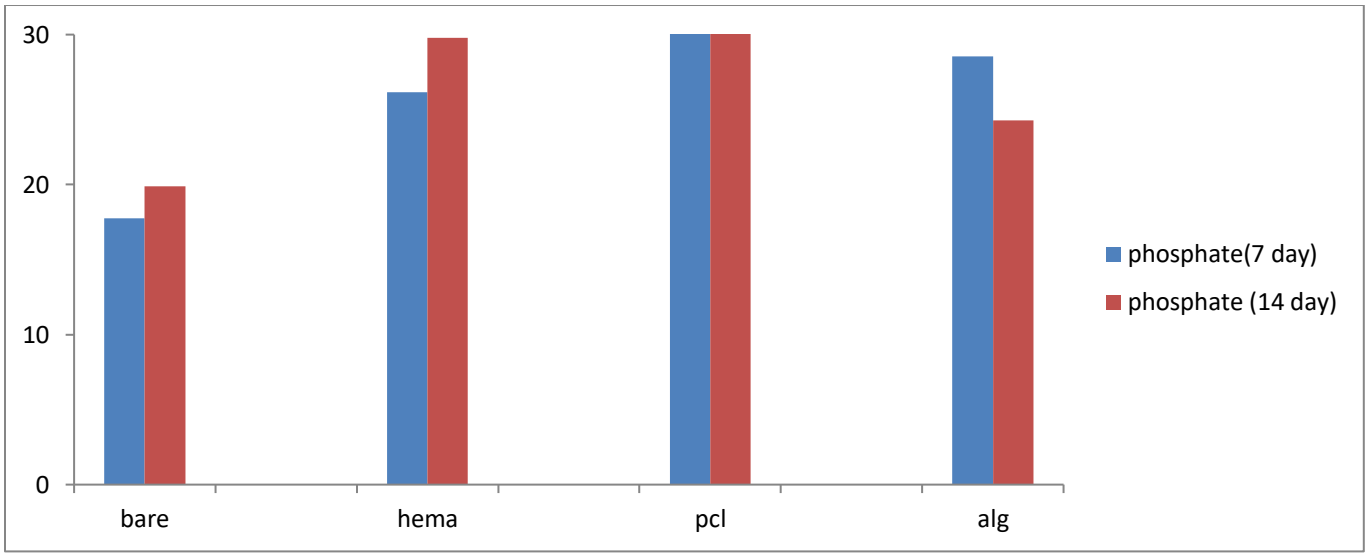

Fig 3.36: Phosphate ion concentration in SBF after 7,14 days

Both Calcium ion concentration and Phosphate ion concentration varied with time and there was no systematic or definite pattern of variation. In case of Ca ion concentration bare Hap pellet was on higher side while for Phosphate it was consistently lower than the other compositions.

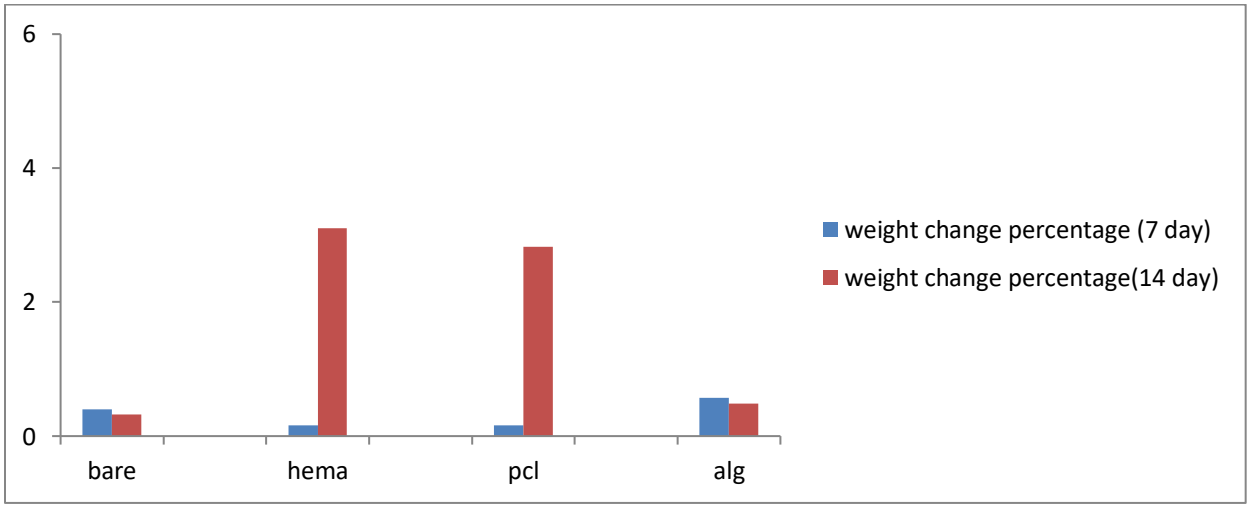

Fig 3.37: Non-dimensionalized weight change plot for composite pellets after 7,14 days in SBF

From the figures, it was evident that the change in weight as a function of time was not also very systematic in nature. In two cases, after 14th day, change in weight was higher than corresponding change, found on 7th day. In case of pure HAp, the change was minimal while for the polymer loaded samples, the values were higher. may be because of the inherent biodegradation of the polymers. The concentrations of ions also revealed a non-uniform pattern of variation which may be due to differential extent of coating of polymers on the Hap substrate.

3.6 Discussions

XRD Analysis :

X ray crystallography of calcined HAp powder reveals that the characteristic peaks corresponding to various crystallographic planes like (300), (112), (211) etc were present which matched with standard JCPDS-ICDD powder diffraction file (PDF no. 09-0432). It has been tried to find out the extent of crystallinity from the height of (300) peak and height of the valley between (300) and (112) planes. From the results, we have seen that calcined HAp powder has around 78% crystallinity whereas for the sintered HAp pellet, it was around 93%. SEM images of sintered pellets also revealed nodular shaped clearly defined grains. The percentage crystallinity of the three composite samples showed little shift from that of the sintered pellet.

FTIR Analysis:

In case of FTIR, attempts were made to identify all the peaks associated with the three hydrogels along with their respective ingredients from which those compositions were prepared. Figures and tabulated data reveal clearly the major peaks associated with individual constituents were retained with little shift in final compositions in all three compositions. The small variations actually confirmed the fact of interaction with one another.

Nano-indentation studies:

Nano-indentation studies have been done for all the samples (unloaded and loaded). Small flat domains were selected through repeated visual inspections and trials. A pre-programmed loading was selected that ensured large number of indentations at a particular load in a pre-identified flat domain. An indentation load of 500 μN was selected for all cases. As per standard protocol, Young's modulus and indentation hardness were observed along with loading-unloading curves.

In most of the cases, as expected, polymeric samples revealed low hardness (less than 1GPa) and stiffness (less than 8GPa) while the corresponding values for HAp were substantially high (6-8 GPa)for hardness and (greater than 100GPa) for stiffness. For the composites, the values are low and comparable to those of polymer. However, both stiffness and hardness showed higher values. It appears that the loaded composite surfaces were covered fully or partially by the corresponding polymers and hence the presence of polymer on test surface influenced the result more than the HAp substrate. From the loading-unloading curves, it was further noticed that there was no major kink in the loading or unloading part which means that no indentation cracks formed. Moreover the plasticity index which is nothing but a ratio of final depth of penetration to maximum depth of penetration was mostly above 0.7 i.e. the material under testing was soft and highly deformable.

TGA Analysis:

TGA curves of pure HAp and polymer loaded HAp have been shown in results. It revealed that pure HAp pellet, when tested up to 1150^0C, did not show any measureable change in mass. However, for the hydrogels, substantial amount of mass loss took place before 350-400^0C. From the curves of the composite pellets, it was evident that they did not follow a similar pattern of loss as a function of temperature but at maximum temperature, all three samples lost substantial mass. (20% for Phema-Aam loaded pellet, 4-5% for the other two).

It indirectly confirms that the hydrogels were loaded in porous HAp, may be in two different forms, a coating on the outer surface and intruded inside the pores. SEM results and Nano-indentation further corroborates this fact.

Scanning Electron Microscopy Images (SEM):

Pure HAp shows a porous structure with clearly defined nodular shaped grains. The pores were observed under SEM and they revealed a size of around 200-500 microns. The extent of porosity was measured through image analysis and found to be around 40-45% which is comparable with the gravimetric data.

In case of all three hydrogel loaded samples, polymers were found to stick to outer layer as well as flakes shaped layers (2D film shaped) of polymers in fragmented form were observed either inside the pores of HAp or surrounding them.

SBF Bioactivity:

Study of the three hydrogel loaded Hap along with unloaded HAp reveal how the samples performed when immersed in SBF, maintained at 37^0C temperature over a period of 14 days and tested intermittently on 7^{th} day and on the 14^{th} day. We can see that calcium and phosphate concentrations changed in SBF in all the four cases with time however the rates were not same. In case of polymer loaded samples, the values of concentration did not reveal any definite, systematic patter. There was a few amount of scatter and fluctuation in the data but when coupled with results of gravimetric analysis, it revealed an interesting fact. As it is already mentioned that hydrogel loading on HAp often formed a non uniform layer of hydrogel on Hap (as is evident from SEM and indirectly manifested in nano-indentation studies), it was expected that those layers would have some effect on the degradation of the samples. The gravimetric analysis revealed that for HAp, the drop (non-dimensionalized) in weight with time was low owing to both dissolution and apatite layer formation, two opposing mechanisms. In case of hydrogel loaded samples, the hydrogels were degradable. So, in addition to the above mentioned two mechanisms (to some extent negating each other), a third yet strong degradation mechanism was present. This was the reason why all the loaded HAp specimen suffered more weight loss than pure HAp on 7 and 14 days.

In this context, it seems worth mentioning that though the three hydrogels showed different swelling and biodegradation properties, in loaded form that distinct difference was not noticed. The non-uniform coverage over HAp substrate, non-uniform loading of hydrogels may be responsible for this discrepancy.

A brief summary highlighting the major observations are mentioned below.

Major Observations:

1. Three different kinds of biodegradable polymers have been developed through thorough process optimization.

2. The biodegradation rates of the three polymers are found to be distinctly different. pHema-pAam shows slow degradation, PVA-Alginate shows fast and PVA-CH-PCL hydrogel is the intermediate one.
3. HAp powder was synthesized using wet chemical route, calcined at 800°C to get more than 75% crystallinity and porous compacts are prepared with controlled porosity of around 45%. The composition and phase purity of HAp was confirmed through standard characterization process.
4. All three biodegradable polymers could be loaded into porous HAp through different process following extensive optimization. TGA confirmed loading was effectively done in all the cases.

   Even after composite preparation, HAp and respective polymers retained their composition. Hemolysis confirmed that all the specimens were hemocompatible.
5. Nano-indentation revealed that HAp samples had stiffness in excess of 100 GPA and hardness of more than 6-7 GPA while the polymeric materials had stiffness in the range of 7-8 GPA and hardness well within 400 MPa. The polymer loaded HAp had stiffness and hardness comparable to those of polymers which may be attributed to the formation of polymers layers over HAp.
6. SEM micrographs revealed that HAp was porous with nodular shaped grains. In case of loaded HAp, polymers formed layers in HAp and also intruded inside the pores and was visible in the form of flakes.
7. Bioactivity study in SBF confirmed that the degradation of loaded samples were faster than that of HAp due to the inherent biodegradation rate of the polymers.
8. Analysis done over the surface confirmed that polymeric materials intruded well into the pores of HAp.

CHAPTER 4:
CONCLUSION

4. Conclusion

The present study developed three different compositions of biodegradable hydrogels with different swelling ratios and biodegradability. These polymers were physically and mechanically characterised and successfully loaded into porous HAp (with around 45% porosity). The loaded composites were subjected to physical, chemical, mechanical and bioactivity studies following standard test protocols. FTIR confirmed that most of the importants peaks of the constituents were retained after loading.

From the details of thermo-gravimetric analysis, it was evident that the hydrogel loaded pellets were able to retain the hydrogels (although at different quantities). The hydrogels were loaded in different methods after systematic optimisation of process parameters. All the hydrogels while loaded on porous Hap, formed non-uniform coating over the HAp surface as well as intruded into the pores as flakes. The results confirmed that polymeric depositions were there inside the pores and cavities of the porous hydroxyapatite.

All the composites were found to be hemocompatible and their stiffness and hardness were higher than the individual polymer compositions. The values of stiffness of these hydrogel loaded Hap samples were comparable to those of human cancellous bone. None of the loaded specimen showed any sign of indentation crack formation while the porous Hap formed indentation cracks during nanoindentation testing because of its inherent brittleness. It was evident that the loaded samples degrade in simulated body fluid along with the formation of apatite layer over them as a function of time. The hydrogels that degrade fast were found to have higher mass loss when they were loaded into Hap and subjected to bioactivity study, particularly after prolonged explosure. Primarily, it can be said that the preliminary results, obtained so far through the present study, hint towards the suitability of these materials for the preparation of bone regeneration scaffolds, particularly for the cancellous bone portion.

CHAPTER 5:

FUTURE SCOPE OF THE WORK

5. Future Scope of Work

Some portions of the study are still being done with results awaited like MTT assay on the composites, FTIR study of Hap sintered at different temperatures, FESEM to understand the minute intricacies in a more comprehensive way. It is envisaged that with the addition of those results, the work can be carried forward with a detailed and controlled study on cell-material interaction over a long range of time domain as well as with in-vivo tests.

CHAPTER 6:
REFERENCES

6. References

1. L. Hench, Biomaterials, 19, 1419-1423 (1998)
2. Meysam Haghshenas, Journal of Magnesium and Alloys, 5 189–201(2017)
3. T. Lei et al., Corros. Sci. 54 270e277. (2012)
4. Zheng et. al, Bioactive Materials, 2, 1- 9 (2017).
5. J. Seal et. al, IOP Conf. Series: Mat. Science and Engg 4,12011(2009).
6. Yar et.al, Int. Journal of Pol. Mat. and Pol. Biomat., ISSN: 0091-4037 (2016).
7. R. Mohapatra et.al, Polymers & Polymer Composites, Vol. 13, No. 8, (2005).
8. Gkioni et.al, Tissue Engineering: Part B Volume 16, Number 6, (2010).
9. Raucci et. al, Jr. of Bio Mat Res A | JUL VOL 106A, ISSUE 7 (2018).
10. Chang et.al, Carbohydrate Polymers 91 7– 13 (2013).
11. Lima et.al, Polym. Adv. Technol., 26 1439–1446 (2015).
12. Rapado et. al, Polimeros, 25(6), 547-555 (2015).
13. Y.F. Zheng et al, Mater. Sci. Eng. R 77 1–34(2014).
14. Y. Xin et al, Surf. Coat. Technol. 203 2554–2557(2009).
15. C. Liu et al, Mater. Sci. Eng. A 456 350–357. (2007).
16. Y.F. Zheng et al, Mater. Sci. Eng. R 77 1e34 (2014).
17. A. Jankovic et al J. Alloys Compd. 624 148e157 (2015).
18. H.Y. Xia et al, Mater. Sci. Eng. C 33 5044e5050 (2013).
19. T. Lei et al, Corros. Sci. 54 270e277. (2012).
20. JL Christopher et al, J Cell Biology.; 172:909–21(2006).
21. S Bhumiratana et al, Biomaterials. 32: 2812–20. (2011).
22. AR Amini et al, Crit Rev Biomed Eng. 40(5): 363–408 (2012).
23. S Bose et al, Trends Biotechnol. 30(10):546–54 (2012).
24. JY Rho et al, Med Eng Phys 20, 92, (1998).
25. S. Weiner et al, Annu Rev Mater Sci 28, 271, (1998).
26. K.J.L. Burg et al , Biomaterials 21, 2347, (2000).

27. R. LeGeros, Clin Orthop Relat Res 395, 81, (2002).

28. J. D. Kretlow et al, Tissue Eng 13, 927, (2007).

29. Y.J. Kim, Pharm. Res., 18, 548-50 (2001).

30. C. Mastschke et al., J Cont.Rel., 85 ,1-15 (2001)

31. G. Wei et al, J Cont. Rel., 83, 65-74 (2002).

32. S. Miyazaki et al, J Cont. Rel., 56 , 75-83 (1998).

33. V. Carelli et al, Int. J Pharm., 179 73-83(1999).

34. J. Habsuda et al, J Polym. Sci. Part A: Polym Chem., 39 1342-52 (2001).